Energy, Mines and Resources Canada

Énergie, Mines et Ressources Canada

CANMET

Canada Centre for Mineral and Energy Technology

Centre canadien de la technologie des minéraux et de l'énergie

Mining Research Laboratories

Laboratoires de recherche minière

Canada

HIGH TEMPERATURE UNIAXIAL AND TRIAXIAL COMPRESSION TESTS ON URL ROCK SAMPLES FROM BOREHOLES 209-021-SV1 AND 209-025-SV2

J.S.O. Lau and B. Gorski August 1990

Mining Research Laboratories
Divisional Report MRL 90-079(TR)

51PP

MICROMEDIA

91-00385/

HIGH TEMPERATURE UNIAXIAL AND TRIAXIAL COMPRESSION TESTS ON URL ROCK SAMPLES FROM BOREHOLES 209-021-SV1 AND 209-025-SV2

by

J.S.O. Lau[1] and B. Gorski[2]

ABSTRACT

A series of ambient room and high temperature uniaxial and triaxial compression tests were conducted on grey granitic core samples obtained from boreholes 209-021-SV1 and 209-025-SV2 located at the 240 level of AECL Research's Underground Research Laboratory (URL). Twelve sets of tests were carried out at three temperatures (18°−25°, 75° and 125° C) and four confining pressures (0, 3.5, 17 and 35 MPa) to study the thermo-mechanical properties of the grey granite.

The failure deviator stress and axial strain at failure were found to increase with increasing confining pressure, but decrease with increasing temperature.

The tangent Young's modulus and pseudo Young's modulus increased with increasing confining pressure at stress levels below approximately 50% of the failure deviator stress. Temperatures up to 125° C had very little effect on these two moduli.

The strength properties of the rock were expressed in terms of the Hoek and Brown failure criterion. The uniaxial compressive strength of the intact rock material, σ_c, decreased only when the temperature was raised from 75° to 125° C. It appears that temperatures up to 125° C had little effect on the material constant, m. The Mohr-Coulomb friction angle, ϕ, decreased and the cohesive strength, c, increased with increasing confining pressure. Temperatures up to 125° C appeared to have no effect on ϕ and c.

Keywords: uniaxial, triaxial, compression, temperature, confining pressure, strength, strain, modulus, Hoek-Brown, Mohr-Coulomb

---

[1]Geotechnical Engineer, AECL Research, on attachment to Canadian Mine Technology Laboratory, Mining Research Laboratories, CANMET, Energy, Mines and Resources Canada, Ottawa, Ontario.

[2]Rock Mechanics and Development Technologist, Canadian Mine Technology Laboratory, Mining Research Laboratories, CANMET, Energy, Mines and Resources Canada, Ottawa, Ontario.

ESSAIS DE COMPRESSION UNIAXIALE ET TRIAXIALE À HAUTE TEMPÉRATURE SUR DES ÉPROUVETTES DE ROCHE DES SONDAGES 209-021-SV1 ET 209-025-SV2 DU LRS

par

J.S.O. Lau[1] et B. Gorski[2]

RÉSUMÉ

On a effectué une série d'essais de compression uniaxiale et triaxiale à la température ambiante et à température élevée sur des carottes de granite gris prélevées dans les trous de sondages 209-021-SV1 et 209-025-SV2 situés au niveau 240 du Laboratoire de recherche souterrain (LRS) de EACL Recherche. On a effectué douze séries d'essais à trois températures différentes (18° – 25°, 75° et 125° C) et à quatre pressions de confinement (0, 3.5, 17 et 35 MPa) pour étudier les propriétés thermomécaniques du granite gris.

On a constaté que la contrainte déviatrice à la rupture et la déformation axiale à la rupture augmentaient en même temps que la pression de confinement, mais diminuaient lorsque la température augmentait.

Le module de Young tangentiel et le pseudo-module de Young augmentaient en même temps que la pression de confinement à des niveaux de contraintes inférieurs à environ 50% de la contrainte déviatrice. Les températures allant jusqu'à 125° C avaient très peu d'effet sur ces deux modules.

Les propriétés de résistance mécanique de ces roches ont été exprimées en fonction du critère de rupture de Hoek et Brown. La résistance à la compression uniaxiale de la

---

[1]Ingénieur en géotechnique, EACL Recherche, affecté au Laboratoire canadien de technologie minière, Laboratories de recherche minière, CANMET, Énergie, Mines et Ressources Canada, Ottawa, Ontario.

[2]Technologue en mécanique des roches et développement, Laboratoire canadien de technologie minière, Laboratoires de recherche minière, CANMET, Énergie, Mines et Ressources Canada, Ottawa, Ontario.

roche intacte, σ_c, ne diminuait que lorsque la température était élevée de 75° à 125° C. Il semble que les températures atteignant 125° C aient eu peu d'effet sur la constante matérielle, m. L'angle de frottement de Mohr-Coulomb, ϕ, diminuait et la résistance au cisaillement, c, augmentait avec la pression de confinement. Les températures allant jusqu'à 125° C n'avaient apparemment aucun effet sur ϕ et sur c.

Mots clés: uniaxiale, triaxiale, compression, température, pression de confinement, résistance mécanique, module, Hoek-Brown, Mohr-Coulomb

CONTENTS

	Page
ABSTRACT	i
RÉSUMÉ	ii
INTRODUCTION	1
SAMPLING AND SPECIMEN PREPARATION	2
DYNAMIC ELASTIC PROPERTIES	2
TEST APPARATUS AND PROCEDURE	3
TESTING PROGRAM	4
RESULTS AND DISCUSSION	4
Test Results	4
Failure Deviator Stress	5
Axial Strain at Failure	5
Tangent Young's Modulus	5
Pseudo Young's Modulus	6
Poisson's Ratio	7
Strength Properties	7
CONCLUSIONS	10
RECOMMENDATIONS	11
ACKNOWLEDGEMENTS	11
REFERENCES	12
APPENDIX A	32

TABLES

No.		
1.	Dimensions, densities and dynamic elastic properties of rock specimens.	13
2.	Results of ambient room and high temperature uniaxial and triaxial compression tests.	14
3.	Tangent Young's moduli at stress levels ranging from 10 to 90% of the failure deviator stress.	16
4.	Pseudo Young's moduli at stress levels ranging from 10 to 90% of the failure deviator stress.	18
5.	Mean values and standard deviations (in brackets) of failure	

deviator stress, axial strains at failure, tangent Young's modulus and pseudo Young's modulus. 20
6. Values of σ_c, m, s, r^2, σ_{cmass} and σ_{tmass} derived from the Hoek and Brown failure criterion. 21
7. Values of the Mohr-Coulomb friction angle ϕ and cohesive strength c. 22

FIGURES

1. Plots of failure deviator stress versus temperature. 23
2. Plots of axial strain at failure versus temperature. 24
3. Plots of mean tangent Young's modulus at the stress level of 50% of $(\sigma_1 - \sigma_3)_f$ versus temperature. 25
4. Plots of mean pseudo Young's modulus at the stress level of 50% of $(\sigma_1 - \sigma_3)_f$ versus temperature. 26
5. Plots of Poisson's ratio versus temperature. 27
6. Hoek and Brown failure envelope for tests conducted at 18° – 25° C. 28
7. Hoek and Brown failure envelope for tests conducted at 75° C. 29
8. Hoek and Brown failure envelope for tests conducted at 125° C. 30
9. Effect of temperature on the Hoek and Brown failure envelope. 31

INTRODUCTION

The Canadian Nuclear Fuel Waste Management Program (CNFWMP) is concerned with the safe, long term disposal of high level nuclear wastes in vaults located at depth in plutonic rock. AECL Research has constructed the Underground Research Laboratory (URL) located near to Lac du Bonnet, Manitoba to provide a representative environment in which to conduct large scale in situ investigations. In support of these investigations, a joint laboratory testing and analysis program has been undertaken by the Canada Centre for Mineral and Energy Technology (CANMET) and AECL Research to provide data on the mechanical properties of the rock mass surrounding the URL excavation under both ambient room and high temperature conditions. This information is required by numerical modellers for input into mechanical models and by engineers for the design of the experiments to be carried out at the URL. The information is also necessary for the development of the geotechnical data base for the URL characterization program.

Series of uniaxial and triaxial compression tests at ambient room and high temperatures were conducted in 1988 and 1989 on core samples of grey granite obtained from boreholes 209-021-SV1 and 209-030-DIL1 located in Room 209 at the 240 level of the URL and the results were reported by Lau et al. (1988) and Lau and Gorski (1989). It was noted that the effect of heating to 125° C on the mechanical properties of the rock can be masked by intrinsic differences in samples obtained from those two boreholes. Rock samples obtained from borehole 209-021-SV1 (trend = 046.38°, plunge = −04.89°), drilled at the northeast side of Room 209, were found to be consistently stronger and stiffer than those obtained from borehole 209-030-DIL1 (trend = 209.92°, plunge = −02.83°), drilled at the southwest side of Room 209. It has been concluded that a meaningful study on the effect of heating on the mechanical properties of the rock can be carried out only if data obtained from boreholes with different orientations and at different locations are treated separately. Consequently, data obtained from those two boreholes are divided accordingly into two sets for the study of thermo-mechanical properties of the grey granite.

Fourteen tests were conducted in the spring of 1990 on samples from boreholes 209-021-SV1 and 209-025-SV2 (trend = 045.97°, plunge = −04.13°) which were drilled at the northeast side of Room 209 to provide additional results to complete the temperature profiles for that data set (trend = northeast, plunge = subhorizontal). This report presents and discusses the results of all the uniaxial and triaxial compression tests that have been carried out on samples obtained from these two boreholes, including data previously reported by Lau et al. (1988) and Lau and Gorski (1989).

SAMPLING AND SPECIMEN PREPARATION

Samples used in these tests were NQ rock cores from boreholes 209-021-SV1 and 209-025-SV2. The rock is a grey, medium- to coarse-grained granite, composed of approximately 30% K-feldspar, 30% plagioclase, 30% or slightly less quartz and 10% or slightly more mafic minerals, mainly biotite. Specimens were prepared in accordance with the procedure described in the Pit Slope Manual Supplement 3-5 (Gyenge and Ladanyi, 1977) and the method suggested by the International Society for Rock Mechanics (Brown, 1981).

The lengths, diameters and bulk densities of the specimens are shown in Table 1. It should be noted that in Table 1, the last number in the specimen identification is the downhole length of the specimen. The lengths of the specimens varied from 95.47 to 117.16 mm and the diameters varied from 44.97 to 45.23 mm, with length to diameter ratios ranging from 2.1 to 2.6.

DYNAMIC ELASTIC PROPERTIES

Prior to the testing, compression (p) and shear (s) wave velocity measurements were made on the rock specimens. The purpose of the p- and s-wave measurements is to estimate various mechanical rock properties non-destructively prior to actual testing. The velocity measurements were made in accordance with the procedures described in the Instruction Manual - Sonic Velocity Equipment (Terrametric, 1980) and the Pit Slope Manual Supplement 3-2 (Gyenge and Herget, 1977). The p- and s-wave velocities were determined using their respective transit times along the longitudinal axes of the specimens. The dynamic elastic constants were computed from the wave velocities using the following equations:

Dynamic Young' modulus of elasticity:

$$E_u = \frac{\rho V_s^2 (3V_p^2 - 4V_s^2)}{V_p^2 - V_s^2} \qquad (1)$$

where E_u = dynamic Young's modulus of elasticity
V_p = compression wave velocity
V_s = shear wave velocity
ρ = bulk density

Dynamic shear modulus:

$$G_u = \rho V_s^2 \tag{2}$$

where G_u = dynamic shear modulus

Dynamic Poisson's ratio:

$$\nu_u = \frac{V_p^2 - 2V_s^2}{2(V_p^2 - V_s^2)} \tag{3}$$

where ν_u = dynamic Poisson's ratio

The p-wave velocity, s-wave velocity, dynamic Young's modulus, dynamic shear modulus and dynamic Poisson's ratio determined for each of the specimens and their mean values and standard deviations (s.d.) are shown in Table 1.

TEST APPARATUS AND PROCEDURE

The apparatus used to carry out the uniaxial and triaxial compression tests was a MTS 815 Rock Mechanics Test System. The MTS system is a servo-hydraulic press consisting of a 2.22 MN rated load cell, load frame, hydraulic power supply, triaxial cell, test controller, test processor, temperature controller and DEC micro PDP 11/73 computer. The triaxial cell is rated up to 200° C and equipped with a heater, heat shroud, thermocouples, three linear variable differential transducers (LVDTs) for the measurement of axial strain and an extensometer with a circumferential kit for the measurement of circumferential strain. For a detailed description of the MTS system and its operation, the reader is referred to the MTS Operation Manual (MTS Systems Corp., 1986) and CANMET Division Report MRL 87-33(INT) (Gorski, 1987).

The procedures used to conduct the uniaxial and triaxial compression tests are described in CANMET Division Reports MRL 89-90(TR) (Lau and Gorski, 1989) and MRL 88-112(TR) (Lau et al., 1988) respectively, and therefore will not be repeated in this report.

TESTING PROGRAM

Testing for this study took place at Canadian Mine Technology Laboratory, Mining Research Laboratories, CANMET, Energy, Mines and Resources Canada in Ottawa between 1988 and 1990. The testing program consisted of a total of twelve sets of tests conducted at the confining pressures of 0.0, 3.5, 17.0 and 35.0 MPa and at the test temperatures of 18° – 25°, 75° and 125° C. Three tests were carried out under the same confining pressure and temperature conditions in each set in order to obtain statistically meaningful mean values. A total of 36 tests were performed. The testing program is summarized in Table 2.

RESULTS AND DISCUSSION

TEST RESULTS

Table 2 summarizes the axial strain at failure, failure deviator stress, tangent Young's modulus and pseudo Young's modulus at a stress level equivalent to 50% of the failure deviator stress, Poisson's ratio, failure angle, θ, and failure characteristics of each of the specimens. Note that measurements of axial strain were made using LVDTs while circumferential strains were measured using a bicycle chain extensometer. The axial strains, presented in Table 2 and illustrated in the stress-strain curves in Appendix A, represent the average of the axial deformations obtained from the three LVDTs. The Poisson's ratio was determined from the ratio of the circumferential to the axial tangent moduli at the stress level equivalent to 50% of the failure deviator stress. The effects of the confining pressure and temperature on the strength and elastic properties of the rock samples will be discussed in the following subsections.

Stress versus strain curves for tests conducted in 1988 and 1989 have been presented in CANMET Division Reports MRL 88-112(TR) and MRL 89-90(TR) and therefore only those for tests conducted in 1990 are presented in Appendix A of this report. These curves were plotted by the use of the DATAPLOT curve fitting software. A cubic spline fit was used for this analysis which employed a third degree equation model of the form:

$$\sigma = a_0 + a_1\varepsilon + a_2\varepsilon^2 + a_3\varepsilon^3 \qquad (4)$$

where σ = stress

ε = strain

and a_0, a_1, a_2 and a_3 are coefficients

FAILURE DEVIATOR STRESS

One of the main objectives of these tests is to study the effects of confining pressure and temperature on the strength of the rock specimens. The failure deviator stresses of the specimens and their mean values are shown in Tables 2 and 5 respectively. Note that in Table 5, the standard deviations are given in brackets. The faliure deviator stresses and their mean values are also plotted against temperature in Figure 1. As expected, the failure deviator stress increased as the confining pressure increased. Temperature appeared to have some effect on the strength of the rock. In both the unconfined condition and at a confining pressure of 3.5 MPa, there was little change in the failure deviator stress as the temperature was raised from room temperature to 75° C. However, when the temperature was further increased to 125° C, reductions of 3% and 7% were observed for the unconfined condition and at a confining pressure of 3.5 MPa respectively. At the higher confining pressures of 17 and 35 MPa, the failure deviator stress decreased continuously as the temperature increased from room temperature to 125° C. At these two confining pressures, the mean failure deviator stress decreased by 6% on heating to 125° C.

AXIAL STRAIN AT FAILURE

The axial strains at failure and their mean values are given in Tables 2 and 5 respectively, and are also plotted versus temperature in Figure 2. They show that the axial strain at failure increased as the confining pressure increased, but decreased with increasing temperature. Reductions of 12%, 9%, 5% and 8% in the axial strain at failure were observed at the confining pressures of 0, 3.5, 17 and 35 MPa respectively when the temperature was raised from room temperature to 125° C.

TANGENT YOUNG'S MODULUS

Tangent Young's moduli for each of the rock specimens were computed from the stress-strain curves (Appendix A) at nine stress levels corresponding to 10, 20, 30, 40, 50, 60, 70, 80 and 90% of the failure deviator stress, $(\sigma_1 - \sigma_3)_f$, and are presented in Table 3. The tangent moduli were determined by substituting the axial strain values at

those nine stress levels into the derivatives of the equations (Equation 4) representing those curves.

The tangent Young's modulus varied at different stress levels. Under the unconfined condition, the tangent modulus increased until approximately 60% of $(\sigma_1 - \sigma_3)_f$ was reached and then decreased until failure. At the confining pressures of 3.5 and 17 MPa, the tangent modulus behaved similarly. However, at 3.5 MPa, the maximum value of tangent modulus was reached at approximately 45% of $(\sigma_1 - \sigma_3)_f$, and at the higher confining pressure of 17 MPa, the maximum value was reached at approximately 20% of $(\sigma_1 - \sigma_3)_f$. At the highest confining pressure of 35 MPa, the tangent modulus decreased slowly with increasing deviator stress.

The tangent modulus increased with increasing confining pressure at stress levels below approximately 50% of $(\sigma_1 - \sigma_3)_f$, especially at low stress levels. The increase was particularly pronounced when the confining pressure was raised from 3.5 to 17 MPa, suggesting that some stress relaxation had occurred in these specimens, resulting in larger deformations and lower modulus values at low confining pressures. At stress levels above 50% of $(\sigma_1 - \sigma_3)_f$, the confining pressure appeared to have no effect on the tangent modulus.

The mean tangent Young's moduli at the stress level of 50% of $(\sigma_1 - \sigma_3)_f$ for the four confining pressures and three test temperatures are shown in Table 5 and were plotted against temperature in Figure 3. The modulus-temperature plots show that temperatures up to 125° C had little effect on the tangent modulus at the confining pressures of 3.5, 17 and 35 MPa. A slight reduction (2%) in the modulus value was observed for the unconfined condition, as the temperature was raised from room temperature to 125° C.

PSEUDO YOUNG'S MODULUS

Actual stress versus axial strain curves for these specimens are nonlinear (see Appendix A). For modelling purposes, these nonlinear curves may be idealized as a series of straight lines joining points corresponding to stress levels of 0.0, 0.1, 0.2, 0.3, 0.4, 0.5, 0.6, 0.7, 0.8, 0.9 and 1.0 times the failure deviator stress. The slope of each of those straight lines is defined as the pseudo Young's modulus. The pseudo Young's moduli of the rock specimens are presented in Table 4. In general, the pseudo moduli are lower than the tangent moduli at stress levels below approximately 40% of $(\sigma_1 - \sigma_3)_f$, but higher at stress levels above approximately 60% of $(\sigma_1 - \sigma_3)_f$. At stress levels between 40% and 60% of $(\sigma_1 - \sigma_3)_f$, the pseudo moduli are similar to the tangent moduli.

The effects of confining pressure and temperature on the pseudo Young's modulus are similar to those on the tangent modulus. The pseudo modulus increased with increasing confining pressure only at stress levels below approximately 50% of $(\sigma_1 - \sigma_3)_f$. The mean pseudo Young's moduli at the stress level of 50% of $(\sigma_1 - \sigma_3)_f$ are shown in Table 5 and plotted against temperature in Figure 4. The plots show that temperatures up to 125° C also had little effect on the pseudo modulus. Only the unconfined conditions exhibited a 2% reduction in the modulus value as the temperature was raised from room temperature to 125° C.

POISSON'S RATIO

The Poisson's ratios obtained from these tests are presented in Table 2 and are also plotted versus temperature in Figure 5. It should be noted that no circumferential strain measurement was made in tests conducted in 1988. Consequently, insufficient data is available to evaluate statistically meaningful values for Poisson's ratio. Nevertheless, the trends of an increase of Poisson's ratio with increasing confining pressure and a slight decrease of Poisson's ratio with increasing temperature are apparent in the plot of Poisson's ratio versus temperature.

STRENGTH PROPERTIES

The strength properties of the intact rock material of these specimens can be expressed in terms of the Hoek and Brown failure criterion. The empirical relationship developed by Hoek and Brown (1980) between the principal stresses associated with the failure of a rock is given as follows:

$$\sigma_1 = \sigma_3 + \sqrt{m\sigma_c\sigma_3 + s{\sigma_c}^2} \tag{5}$$

where σ_1 = major principal stress at failure
σ_3 = minor principal stress applied to the rock sample
σ_c = uniaxial compressive strength of the intact rock material in the specimen
m and s are constants

The values of m and s depend on the properties of the rock and the extent to which the rock has been broken before being subjected to the principal stresses σ_1 and σ_3. For

these specimens which are intact rocks, $s = 1$, and the uniaxial compressive strength, σ_c, and the material constant, m, can be computed by using the following equations:

$$\sigma_c^2 = \frac{\sum y_i}{n} - \left[\frac{\sum x_i y_i - \frac{\sum x_i \sum y_i}{n}}{\sum x_i^2 - \frac{(\sum x_i)^2}{n}}\right]\frac{\sum x_i}{n} \tag{6}$$

$$m = \frac{1}{\sigma_c}\left[\frac{\sum x_i y_i - \frac{\sum x_i \sum y_i}{n}}{\sum x_i^2 - \frac{(\sum x_i)^2}{n}}\right] \tag{7}$$

where $x = \sigma_3$

$y = (\sigma_1 - \sigma_3)^2$

n = total number of data pairs x_i and y_i

The coefficient of determination r^2 is given by:

$$r^2 = \frac{\left[\sum x_i y_i - \frac{\sum x_i \sum y_i}{n}\right]^2}{\left[\sum x_i^2 - \frac{(\sum x_i)^2}{n}\right]\left[\sum y_i^2 - \frac{(\sum y_i)^2}{n}\right]} \tag{8}$$

The closer the value of r^2 is to 1.00, the better the fit between Equation 5 and the test data is.

The Hoek and Brown failure envelopes generated using Equation 5 for tests conducted at the temperatures of $18° - 25°$, 75° and 125° C are shown in Figures 6, 7 and 8 respectively. The values of σ_c, m and r^2 derived from these tests, computed by using Equations 6, 7 and 8, are presented in Table 6. The coefficient of determination, r^2, was found to range from 0.9857 to 0.9957, indicating that the fit of Equation 5 to the data was good. From Table 6, it can be seen that there was little change in σ_c (from 203 to 204 MPa) when the temperature increased from $18° - 25°$ to 75° C. However, when the temperature was raised to 125° C, σ_c decreased by 6% to 191 MPa. The m value was only slightly affected by heating, decreasing from 36.47 to 32.79 as the temperature increased from $18° - 25°$ to 75° C, and then increasing to 34.52 at the temperature of 125° C. In Figure 9, all three failure envelopes are plotted. It shows a slight decrease in the strength of the rock with increasing temperature.

Hoek (1990) suggests that the uniaxial compressive strength of the rock mass, σ_{cmass}, can be computed by substituting $\sigma_3 = 0$ into Equation 5:

$$\sigma_{cmass} = \sqrt{s}\sigma_c \tag{9}$$

The uniaxial tensile strength of the rock mass, σ_{tmass}, can be calculated by substituting $\sigma_1 = 0$ into Equation 5 and solving the resulting quadratic equation:

$$\sigma_{tmass} = \frac{\sigma_c}{2}(m - \sqrt{m^2 + 4s}) \tag{10}$$

The values of σ_{cmass} and σ_{tmass} derived from these tests are given in Table 6. It can be seen that there is a 6% reduction in the uniaxial compressive strength of the rock mass when the temperature was raised from room temperature to 125° C. However, temperatures up to 125° C appeared to have no effect on the uniaxial tensile strength of the rock mass.

Principal stress circles determined using the Hoek and Brown failure criterion can be used to generate Mohr failure envelopes for these tests (Hoek and Brown, 1980; Lau and Gorski, 1989). Hoek (1990) also suggests the use of the following equations to determine the equivalent values for the Mohr-Coulomb friction angle, ϕ, and cohesive strength, c.

$$\sigma_n = \sigma_3 + \frac{(\sigma_1 - \sigma_3)^2}{2(\sigma_1 - \sigma_3) + \frac{1}{2}m\sigma_c} \tag{11}$$

where σ_n = normal stress

$$\tau = (\sigma_n - \sigma_3)\sqrt{1 + \frac{m\sigma_c}{2(\sigma_1 - \sigma_3)}} \tag{12}$$

$$\phi = 90 - arcsin\left(\frac{2\tau}{\sigma_1 - \sigma_3}\right) \tag{13}$$

$$c = \tau - \sigma_n tan\phi \tag{14}$$

Table 7 presents the Mohr-Coulomb friction angles and cohesive strengths computed by using Equations 11 to 14. The friction angle was found to decrease but the cohesive strength to increase with increasing confining pressure as expected. Temperatures up to 125° C appeared to have no effect on both ϕ and c.

CONCLUSIONS

The results of these tests have provided some thermo-mechanical data as well as some insight into the behaviour of the grey granite at the northeast side of Room 209 at the 240 level of the URL with a northeast/subhorizontal (trend/plunge) orientation. Some reduction in rock strength can occur when the temperature is raised up to 125° C. The deformability of the rock should not be affected by the increase of temperature at confining pressures equivalent to the overburden pressure at the 240 level of the URL. From the results, the following conclusions can be made.

The failure deviator stress increased as the confining pressure increased, but decreased as the temperature increased. Reductions of 3, 7 , 6 and 6% in the mean failure deviator stress were observed at confining pressures of 0, 3.5, 17 and 35 MPa respectively, when the temperature was raised from room temperature to 125° C.

The axial strain at failure increased with increasing confining pressure, but decreased with increasing temperature. The mean axial strains at failure decreased by 12, 9, 5 and 8% at confining pressures of 0, 3.5, 17 and 35 MPa respectively, when the temperature increased from room temperature to 125° C.

At stress levels below approximately 50% of the failure deviator stress, the tangent Young's modulus and the pseudo Young's modulus increased as the confining pressure increased. The increase was particularly pronounced at low confining pressures and at low stress levels. At stress levels above 50% of the failure deviator stress, the confining pressure appeared to have no effect on the moduli. Temperatures up to 125° C were found to have very little effect on both the tangent modulus and the pseudo modulus, with only a slight 2% reduction in the modulus values for the unconfined condition.

The strength properties of the rock specimens are expressed in terms of the Hoek and Brown failure criterion. The uniaxial compressive strength of the intact rock material, σ_c, was found to decrease by 6% when the temperature increased from 75° to 125°

C. However, little change in σ_c was observed when the temperature was raised from room temperature to 75° C. Temperatures up to 125° C appeared to have no effect on the material constant, m.

The uniaxial compressive strength of the rock mass, σ_{cmass}, also decreased by 6% only when the temperature increased from 75° to 125° C. The uniaxial tensile strength of the rock mass, σ_{tmass}, appeared not to be affected by heating up to 125° C.

Mohr-Coulomb friction angles and cohesive strengths of the rock were computed by using equations suggested by Hoek. The friction angle, ϕ, decreased and the cohesive strength, c, increased with increasing confining pressure. Both ϕ and c appeared to be insensitive to the increase of temperatures up to 125° C.

RECOMMENDATIONS

One of the main rock mechanics issues related to the construction and operation of the URL is experimentally identifying the temperature-dependent strength and deformation characteristics of the host rock. This high temperature uniaxial and triaxial compression testing program has addressed this issue and is recommended for the URL characterization program during the operating phase of the URL and for any future site selection program if the disposal concept is deemed acceptable.

Ambient room temperature and high temperature tension tests should also be included in the testing program in order to obtain more accurate values of σ_c and m in the Hoek and Brown failure criterion.

Although results obtained from this testing program have shed some light on the thermo-mechanical properties of the URL rock samples, some questions remain to be answered. What are the scale effects on the thermo-mechanical properties of the URL rock samples? What are the effects of moisture on the thermo-mechanical properties? Will the rock behave the same way at very high confining pressure? These questions should be addressed to in the future.

ACKNOWLEDGEMENTS

The authors wish to express their thanks to R. Jackson of CANMET for reviewing this report and making several helpful suggestions. Gratitude is expressed to J. Folta of

CANMET for the preparation of specimens from borehole 209-025-SV2 and for carrying out the compression wave and shear wave velocities measurements on those specimens.

REFERENCES

Brown, E.T. (1981), "Rock characterization testing and monitoring, ISRM suggested methods", International Society for Rock Mechanics, the Commission on Testing Methods, Pergamon, 211 p.

Gorski, B. (1987), "Post-failure uniaxial strength determinations using a servo-hydraulic test system", Division Report MRL 87-33(INT), CANMET, Energy, Mines and Resources Canada, 77 p.

Gyenge, M. and Herget, G. (1977), "Pit slope manual supplement 3-2 - laboratory tests for design parameters", CANMET, Report 77-26, 74 p.

Gyenge, M. and Ladanyi, B. (1977), "Pit slope manual supplement 3-5 - sampling and specimen preparation", CANMET, Report 77-29, 30 p.

Hoek, E. (1990), "Estimating Mohr-Coulomb friction and cohesion values from the Hoek-Brown failure criterion", Int. J. Rock Mech. Min. Sci. & Geomech. Abstr., Vol. 27, No. 3, p. 227-229.

Hoek, E. and Brown, E.T. (1980), "Underground excavations in rock", The institution of Mining and Metallurgy, London, 527 p.

Lau, J.S.O., Jackson, R. and Gorski, B. (1988), "High temperature triaxial tests on rock samples from boreholes 209-021-SV1 and 209-030-DIL1, Lac du Bonnet, Manitoba", Division Report MRL 88-112(TR), CANMET, Energy, Mines and Resources Canada, 57 p.

Lau, J.S.O. and Gorski, B. (1989), "High temperature uniaxial compression tests on URL rock samples from boreholes 209-021-SV1 and 209-030-DIL1", Divisional Report MRL 89-90(TR), CANMET, Energy, Mines and Resources Canada, 68 p.

MTS Systems Corporation (1986), "Operation manual for 815 rock mechanics test systems", MTS Systems Corp., Minneapolis, Minnesota, U.S.A.

Terrametrics (1980), "Instruction manual - sonic velocity equipment", Terrametrics, Inc., Golden, Colorado, U.S.A., 17 p.

Table 1. Dimensions, densities and dynamic elastic properties of rock specimens.

Specimen identification	Length (mm)	Diameter (mm)	Bulk density (Mg/m^3)	P-wave velocity (km/s)	S-wave velocity (km/s)	Dynamic Young's modulus (GPa)	Dynamic shear modulus (GPa)	Dynamic Poisson's ratio
209-021-SV1-0.44	96.53	44.99	2.63	4.858	2.728	49.77	19.60	0.27
209-021-SV1-0.54	96.98	44.97	2.62	4.930	2.687	48.67	18.88	0.29
209-021-SV1-0.66	95.47	44.99	2.63	4.653	2.728	48.55	19.61	0.24
209-021-SV1-0.76	97.09	45.01	2.64	5.132	2.886	55.78	21.98	0.27
209-021-SV1-0.89	115.77	45.00	2.64	4.830	3.051	57.44	24.59	0.17
209-021-SV1-1.01	117.16	45.02	2.64	4.919	2.997	57.12	23.71	0.21
209-021-SV1-1.13	106.87	45.02	2.64	4.777	2.784	50.92	20.48	0.24
209-021-SV1-1.24	109.63	45.00	2.65	4.934	2.924	55.65	22.64	0.23
209-021-SV1-1.35	107.38	45.00	2.65	4.897	2.861	53.83	21.69	0.24
209-021-SV1-1.47	111.74	45.03	2.64	4.761	2.840	52.15	21.31	0.22
209-021-SV1-1.58	98.94	45.05	2.64	4.663	2.726	48.75	19.65	0.24
209-021-SV1-1.69	96.32	45.10	2.63	4.823	2.838	52.41	21.21	0.24
209-021-SV1-1.79	100.13	45.11	2.64	4.775	2.752	50.03	19.99	0.25
209-021-SV1-4.11	105.65	45.07	2.63	5.187	2.949	57.70	22.88	0.26
209-021-SV1-4.23	106.98	45.09	2.63	4.839	2.795	51.34	20.54	0.25
209-021-SV1-4.34	105.80	45.10	2.63	4.998	2.895	55.01	22.05	0.25
209-021-SV1-4.45	108.06	45.04	2.63	4.711	2.732	48.93	19.62	0.25
209-021-SV1-4.62	105.86	45.20	2.62	4.739	2.761	49.65	19.97	0.24
209-021-SV1-4.73	108.44	45.16	2.63	4.880	2.814	52.12	20.83	0.25
209-021-SV1-4.84	106.43	45.09	2.64	5.300	2.793	53.86	20.59	0.31
209-021-SV1-4.96	106.49	45.09	2.64	5.515	2.809	55.20	20.83	0.32
209-021-SV1-5.40	112.83	45.23	2.62	5.103	2.941	56.70	22.66	0.25
209-021-SV1-5.518	110.77	45.13	2.63	4.837	2.811	51.76	20.79	0.24
209-021-SV1-5.639	108.54	45.12	2.63	4.485	2.714	46.91	19.36	0.21
209-021-SV1-5.760	108.71	45.12	2.63	4.706	2.795	50.43	20.54	0.23
209-021-SV1-5.880	109.78	45.12	2.64	4.555	2.758	48.63	20.09	0.21
209-025-SV2-3.450	100.73	45.10	2.63	4.663	2.730	48.58	19.60	0.24
209-025-SV2-3.565	108.91	45.08	2.63	4.715	2.836	51.47	21.16	0.22
209-025-SV2-12.256	106.42	45.05	2.63	4.950	2.743	50.59	19.79	0.28
209-025-SV2-12.367	101.45	45.05	2.63	4.854	2.720	49.46	19.46	0.27
209-025-SV2-12.565	108.05	45.03	2.63	4.934	2.749	50.69	19.88	0.27
209-025-SV2-12.680	105.08	45.09	2.63	4.820	2.765	50.47	20.11	0.25
209-025-SV2-12.796	109.65	45.02	2.64	4.852	2.855	53.17	21.53	0.24
209-025-SV2-12.913	105.46	45.01	2.63	5.195	2.850	54.90	21.37	0.28
209-025-SV2-13.738	104.22	44.99	2.63	5.011	2.779	51.92	20.31	0.28
209-025-SV2-15.552	104.83	45.00	2.63	4.992	2.723	50.24	19.50	0.29
Mean			2.63	4.883	2.809	51.97	20.80	0.25
Standard deviation			0.01	0.208	0.086	2.93	1.31	0.03

Table 2. Results of ambient room and high temperature uniaxial and triaxial compression tests.

Specimen Identification	Confining Pressure (MPa)	Temp. (deg C.)	Total Axial Strain (%)	Failure Deviator Stress (MPa)	Tangent Young's Modulus (GPa)	Pseudo Young's Modulus (GPa)	Poisson's Ratio	θ (deg.)	Failure characteristics
209-021-SV1-4.11	0.0	25	0.418	189	66.25	65.29	0.36		multiple vertical cracks
209-021-SV1-4.23	0.0	25	0.396	182	64.23	63.12	0.23		multiple vertical cracks
209-021-SV1-5.40	0.0	25	0.345	186	66.09	65.31	0.54		multiple vertical cracks
209-021-SV1-4.34	0.0	75	0.355	178	64.94	63.82	0.25		multiple vertical cracks
209-021-SV1-4.45	0.0	75	0.353	190	67.40	66.51	0.28		multiple vertical cracks
209-021-SV1-4.96	0.0	75	0.348	190	66.38	65.59	0.29		multiple vertical cracks
209-021-SV1-4.62	0.0	125	0.345	180	64.73	63.62	0.28		multiple vertical cracks
209-021-SV1-4.73	0.0	125	0.334	177	63.92	62.82	0.28		multiple vertical cracks
209-021-SV1-4.84	0.0	125	0.343	182	63.96	62.96	0.26		multiple vertical cracks
209-021-SV1-0.44	3.5	18	0.487	266	70.13	70.18			multiple vertical cracks
209-021-SV1-0.54	3.5	20	0.464	255	69.20	69.32			multiple vertical cracks
209-025-SV2-3.450	3.5	21	0.469	264	70.89	71.15	0.34		multiple vertical cracks
209-021-SV1-0.89	3.5	75	0.433	267	75.00	75.15			fragments, conical top and bottom ends
209-021-SV1-1.79	3.5	75	0.459	269	70.65	70.85		70	2 fragments, curved fracture
209-025-SV2-12.367	3.5	75	0.441	253	72.99	73.23	0.32		multiple cracks
209-021-SV1-1.24	3.5	125	0.440	246	69.86	69.64		65	3 fragments, curved fracture, wedge-shaped bottom end
209-021-SV1-5.518	3.5	125	0.428	246	72.84	72.92	0.25		multiple vertical cracks
209-025-SV2-12.913	3.5	125	0.420	240	71.04	71.01	0.27		multiple vertical cracks

Table 2 - (Cont'd)

Specimen Identification	Confining Pressure (MPa)	Temp. (deg C.)	Total Axial Strain (%)	Failure Deviator Stress (MPa)	Tangent Young's Modulus (GPa)	Pseudo Young's Modulus (GPa)	Poisson's Ratio	θ (deg.)	Failure characteristics
209-021-SV1-0.66	17.0	21	0.691	429	71.18	72.13		65	2 fragments, curved fracture
209-021-SV1-0.76	17.0	19	0.675	423	73.39	74.55		67	2 fragments, shear fracture
209-025-SV2-3.565	17.0	21	0.685	413	72.28	73.53	0.39	67	2 fragments, curved fracture
209-021-SV1-1.01	17.0	75	0.695	423	71.37	72.56		65	2 fragments, curved fracture
209-025-SV2-12.565	17.0	75	0.634	390	71.64	72.73	0.33	69	2 fragments, curved fracture
209-025-SV2-12.680	17.0	75	0.668	397	70.48	71.62	0.35		2 fragments, wedge-shaped bottom end
209-021-SV1-1.35	17.0	125	0.666	402	71.03	72.17		70	2 fragments, shear fracture
209-021-SV1-5.639	17.0	125	0.626	393	73.23	74.44	0.34	74	2 fragments,irregular fracture
209-025-SV2-13.738	17.0	125	0.663	392	69.99	71.10	0.33		2 fragments, wedge-shaped bottom end
209-021-SV1-1.58	35.0	22	0.851	543	71.75	73.32		68	2 fragments, curved fracture
209-021-SV1-1.69	35.0	22	0.902	560	69.73	71.27			vertical cracks, wedge-shaped bottom end
209-025-SV2-12.256	35.0	21	0.849	526	71.46	73.03	0.34	64	2 fragments, curved fracture
209-021-SV1-1.13	35.0	75	0.880	538	69.15	70.61			2 fragments, wedge-shaped top end
209-021-SV1-5.880	35.0	75	0.855	524	70.40	71.80	0.34	65	2 fragments, curved fracture
209-025-SV2-12.796	35.0	75	0.812	505	71.34	72.81	0.36	70	2 fragments, curved fracture
209-021-SV1-1.47	35.0	125	0.829	518	69.64	71.08		64	3 fragments, curved fracture, wedge-shaped bottom end
209-021-SV1-5.760	35.0	125	0.766	506	72.91	74.51	0.30	70	2 fragments, curved fracture
209-025-SV2-15.552	35.0	125	0.797	515	70.99	72.38	0.33	70	2 fragments, shear fracture

Table 3. Tangent Young's moduli at stress levels ranging from 10 to 90 % of the failure deviator stress.

Specimen Identification	σ_3 (MPa)	Temp. (deg C.)	Tangent Young's Modulus (GPa)								
			10 %	20 %	30 %	40 %	50 %	60 %	70 %	80 %	90 %
209-021-SV1-4.11	0.0	25	37.24	51.03	59.21	63.98	66.25	66.36	64.33	59.86	50.36
209-021-SV1-4.23	0.0	25	37.96	50.07	57.25	61.73	64.23	65.03	64.23	61.75	54.77
209-021-SV1-5.40	0.0	25	39.82	53.35	60.52	64.25	66.09	66.30	64.89	61.73	54.72
209-021-SV1-4.34	0.0	75	38.49	50.93	57.99	62.44	64.94	65.78	65.05	62.68	54.93
209-021-SV1-4.45	0.0	75	41.45	54.12	61.11	65.31	67.40	67.61	65.98	62.32	54.29
209-021-SV1-4.96	0.0	75	44.93	55.92	61.21	64.57	66.38	66.79	65.85	63.47	56.44
209-021-SV1-4.62	0.0	125	38.74	50.49	57.73	62.24	64.73	65.51	64.65	62.07	54.52
209-021-SV1-4.73	0.0	125	39.65	50.84	57.31	61.48	63.92	64.89	64.46	62.61	55.81
209-021-SV1-4.84	0.0	125	39.53	50.95	57.56	61.69	63.96	64.62	63.74	61.22	54.55
209-021-SV1-0.44	3.5	18	54.24	63.82	67.89	69.92	70.13	68.55	65.01	59.02	47.93
209-021-SV1-0.54	3.5	20	54.45	63.68	67.38	69.16	69.20	67.52	63.92	57.94	46.92
209-025-SV2-3.450	3.5	21	58.47	67.11	69.95	71.17	70.89	69.09	65.59	60.01	49.32
209-021-SV1-0.89	3.5	75	62.38	70.48	73.58	75.05	75.00	73.44	70.24	65.05	54.55
209-021-SV1-1.79	3.5	75	59.13	66.74	69.54	70.81	70.65	69.06	65.89	60.82	51.05
209-025-SV2-12.367	3.5	75	61.55	68.06	71.60	73.19	72.99	70.97	66.94	60.33	49.53
209-021-SV1-1.24	3.5	125	53.67	62.44	66.75	69.14	69.86	68.99	66.42	61.89	51.44
209-021-SV1-5.518	3.5	125	56.55	66.96	70.99	72.73	72.84	71.34	68.09	62.70	53.75
209-025-SV2-12.913	3.5	125	57.25	64.55	68.61	70.70	71.04	69.67	66.43	60.95	51.59

Table 3 - (Cont'd)

Specimen Identification	σ_3 (MPa)	Temp. (deg C.)	Tangent Young's Modulus (GPa)								
			10 %	20 %	30 %	40 %	50 %	60 %	70 %	80 %	90 %
209-021-SV1-0.66	17.0	21	71.85	73.90	73.84	72.95	71.18	68.45	64.60	59.34	50.94
209-021-SV1-0.76	17.0	19	74.35	76.82	76.66	75.54	73.39	70.09	65.42	58.93	49.04
209-025-SV2-3.565	17.0	21	75.94	76.40	75.97	74.62	72.28	68.83	64.03	57.43	47.94
209-021-SV1-1.01	17.0	75	73.82	75.19	74.85	73.60	71.37	68.02	63.34	56.89	46.98
209-025-SV2-12.565	17.0	75	73.81	74.71	74.66	73.65	71.64	68.51	64.04	57.82	48.65
209-025-SV2-12.680	17.0	75	73.21	73.93	73.74	72.60	70.48	67.24	62.66	56.30	46.96
209-021-SV1-1.35	17.0	125	73.47	74.12	74.13	73.12	71.03	67.72	62.94	56.21	46.29
209-021-SV1-5.639	17.0	125	76.74	77.20	76.79	75.49	73.23	69.89	65.25	58.92	49.87
209-025-SV2-13.738	17.0	125	72.38	73.21	73.10	72.05	69.99	66.82	62.30	56.00	46.84
209-021-SV1-1.58	35.0	22	78.57	79.16	77.25	74.80	71.75	67.98	63.34	57.57	48.84
209-021-SV1-1.69	35.0	22	78.26	77.30	75.23	72.73	69.73	66.16	61.87	56.68	49.43
209-025-SV2-12.256	35.0	21	79.72	78.57	76.85	74.51	71.46	67.59	62.70	56.45	47.93
209-021-SV1-1.13	35.0	75	76.50	75.89	74.21	71.99	69.15	65.58	61.14	55.54	47.44
209-021-SV1-5.880	35.0	75	77.04	76.35	75.05	73.09	70.40	66.88	62.33	56.44	48.32
209-025-SV2-12.796	35.0	75	78.74	77.81	76.30	74.17	71.34	67.70	63.07	57.15	49.02
209-021-SV1-1.47	35.0	125	77.06	76.17	74.57	72.42	69.64	66.14	61.76	56.23	48.84
209-021-SV1-5.760	35.0	125	82.29	80.69	78.61	76.04	72.91	69.11	64.50	58.85	51.41
209-025-SV2-15.552	35.0	125	78.23	77.24	75.74	73.67	70.99	67.60	63.34	57.98	50.78

Table 4. Pseudo Young's moduli at stress levels ranging from 10 to 90 % of the failure deviator stress.

Specimen Identification	σ_3 (MPa)	Temp. (deg C.)	Pseudo Young's Modulus (GPa)								
			10 %	20 %	30 %	40 %	50 %	60 %	70 %	80 %	90 %
209-021-SV1-4.11	0.0	25	20.29	44.34	55.38	61.80	65.29	66.48	65.52	62.30	55.84
209-021-SV1-4.23	0.0	25	20.30	44.34	53.85	59.64	63.12	64.76	64.77	63.13	59.19
209-021-SV1-5.40	0.0	25	27.15	47.02	57.23	62.55	65.31	66.33	65.73	63.46	58.88
209-021-SV1-4.34	0.0	75	26.75	45.17	54.65	60.37	63.82	65.49	65.55	64.01	59.86
209-021-SV1-4.45	0.0	75	28.07	48.34	57.82	63.38	66.51	67.65	66.95	64.32	59.03
209-021-SV1-4.96	0.0	75	30.45	51.30	58.71	63.02	65.59	66.70	66.43	64.78	60.93
209-021-SV1-4.62	0.0	125	29.95	44.87	54.31	60.14	63.62	65.25	65.21	63.50	59.21
209-021-SV1-4.73	0.0	125	30.00	45.67	54.24	59.53	62.82	64.52	64.79	63.66	60.21
209-021-SV1-4.84	0.0	125	29.74	45.66	54.44	59.78	62.96	64.42	64.31	62.62	58.65
209-021-SV1-0.44	3.5	18	38.34	59.93	66.02	69.06	70.18	69.50	66.94	62.20	54.09
209-021-SV1-0.54	3.5	20	40.34	59.94	65.69	68.42	69.32	68.51	65.88	61.11	52.97
209-025-SV2-3.450	3.5	21	40.58	63.91	68.66	70.68	71.15	70.12	67.48	62.96	55.37
209-021-SV1-0.89	3.5	75	49.67	67.35	72.16	74.44	75.15	74.35	71.98	67.80	60.62
209-021-SV1-1.79	3.5	75	46.23	63.85	68.26	70.29	70.85	69.98	67.60	63.50	56.64
209-025-SV2-12.367	3.5	75	46.62	65.23	69.99	72.54	73.23	72.13	69.12	63.82	55.30
209-021-SV1-1.24	3.5	125	44.32	58.62	64.75	68.09	69.64	69.56	67.84	64.31	57.53
209-021-SV1-5.518	3.5	125	45.40	62.32	69.28	72.00	72.92	72.23	69.86	65.56	58.68
209-025-SV2-12.913	3.5	125	42.79	61.37	66.74	69.80	71.01	70.50	68.20	63.87	56.75

Table 4 - (Cont'd)

Specimen Identification	σ_3 (MPa)	Temp. (deg C.)	Pseudo Young's Modulus (GPa)								
			10 %	20 %	30 %	40 %	50 %	60 %	70 %	80 %	90 %
209-021-SV1-0.66	17.0	21	64.60	73.41	73.94	73.46	72.13	69.89	66.61	62.06	55.65
209-021-SV1-0.76	17.0	19	65.15	76.26	76.82	76.18	74.55	71.83	67.86	62.30	54.38
209-025-SV2-3.565	17.0	21	69.33	76.25	76.26	75.37	73.53	70.64	66.53	60.85	52.92
209-021-SV1-1.01	17.0	75	69.81	74.87	75.10	74.30	72.56	69.78	65.78	60.23	52.35
209-025-SV2-12.565	17.0	75	70 88	74.34	74.76	74.23	72.73	70.17	66.37	61.05	53.53
209-025-SV2-12.680	17.0	75	70.13	73.65	73.91	73.25	71.62	68.95	65.05	59.60	51.91
209-021-SV1-1.35	17.0	125	74.17	73.74	74.21	73.72	72.17	69.47	65.44	59.71	51.49
209-021-SV1-5.639	17.0	125	79.35	77.04	77.07	76.22	74.44	71.64	67.67	62.20	54.63
209-025-SV2-13.738	17.0	125	74.45	72.28	73.23	72.65	71.10	68.50	64.66	59.27	51.66
209-021-SV1-1.58	35.0	22	74.38	79.46	78.24	76.07	73.32	69.91	65.72	60.52	53.63
209-021-SV1-1.69	35.0	22	74.70	78.08	76.29	74.01	71.27	67.98	64.06	59.33	53.42
209-025-SV2-12.256	35.0	21	84.41	79.19	77.75	75.73	73.03	69.58	65.21	59.65	52.40
209-021-SV1-1.13	35.0	75	74.46	76.44	75.09	73.14	70.61	67.42	63.42	58.40	51.87
209-021-SV1-5.880	35.0	75	80.20	76.75	75.75	74.12	71.80	68.70	64.67	59.46	52.60
209-025-SV2-12.796	35.0	75	78.54	78.32	77.10	75.28	72.81	69.58	65.45	60.19	53.32
209-021-SV1-1.47	35.0	125	74.42	76.74	75.41	73.54	71.08	67.94	64.01	59.06	52.72
209-021-SV1-5.760	35.0	125	82.51	81.54	79.69	77.37	74.51	71.05	66.86	61.73	55.34
209-025-SV2-15.552	35.0	125	80.03	77.78	76.53	74.75	72.38	69.35	65.53	60.73	54.59

Table 5. Mean values and standard deviations (in brackets) of failure deviator stress, axial strain at failure, tangent Young's modulus and pseudo Young's modulus.

Confining pressure (MPa)	Temperature (° C)	Mean failure deviator stress (MPa)	Mean axial strain at failure (%)	Mean tangent Young's modulus (GPa)	Mean pseudo Young's modulus (GPa)
0.0	25	185.7 (3.5)	0.386 (0.037)	65.52 (1.12)	64.57 (1.26)
	75	186.0 (6.9)	0.352 (0.004)	66.24 (1.24)	65.31 (1.37)
	125	179.7 (2.5)	0.341 (0.006)	64.20 (0.46)	63.13 (0.43)
3.5	18-21	261.7 (5.9)	0.473 (0.012)	70.07 (0.85)	70.22 (0.92)
	75	263.0 (8.7)	0.444 (0.013)	72.88 (2.18)	73.08 (2.15)
	125	244.0 (3.5)	0.429 (0.010)	71.25 (1.50)	71.19 (1.65)
17.0	19-21	421.7 (8.1)	0.684 (0.008)	72.28 (1.11)	73.40 (1.22)
	75	403.3 (17.4)	0.666 (0.031)	71.16 (0.61)	72.30 (0.60)
	125	395.7 (5.5)	0.652 (0.002)	71.42 (1.65)	72.56 (1.71)
35.0	21-22	543.0 (17.0)	0.867 (0.030)	70.98 (1.09)	72.54 (1.11)
	75	522.3 (16.6)	0.849 (0.034)	70.30 (1.10)	71.74 (1.10)
	125	513.0 (6.2)	0.797 (0.032)	71.18 (1.64)	72.66 (1.73)

Table 6. Values of σ_c, m, s, r^2, σ_{cmass} and σ_{tmass} derived from the Hoek and Brown failure criterion.

Test Temperature (°C.)	Number of specimens	σ_c (MPa)	m	s	r^2	σ_{cmass} (MPa)	σ_{tmass} (MPa)
18-25	12	203	36.47	1.00	0.9891	203	5.56
75	12	204	32.79	1.00	0.9857	204	6.22
125	12	191	34.52	1.00	0.9957	191	5.53

Table 7. Values of the Mohr-Coulomb friction angle ϕ and cohesive strength c.

Confining pressure (MPa)	Test temperature (°C)	Number of specimens	ϕ	c (MPa)
0.0	25	3	65°	20
	75	3	64°	21
	125	3	64°	20
3.5	18-21	3	61°	27
	75	3	60°	30
	125	3	61°	26
17.0	19-21	3	55°	44
	75	3	54°	43
	125	3	54°	42
35.0	21-22	3	51°	54
	75	3	50°	55
	125	3	50°	53

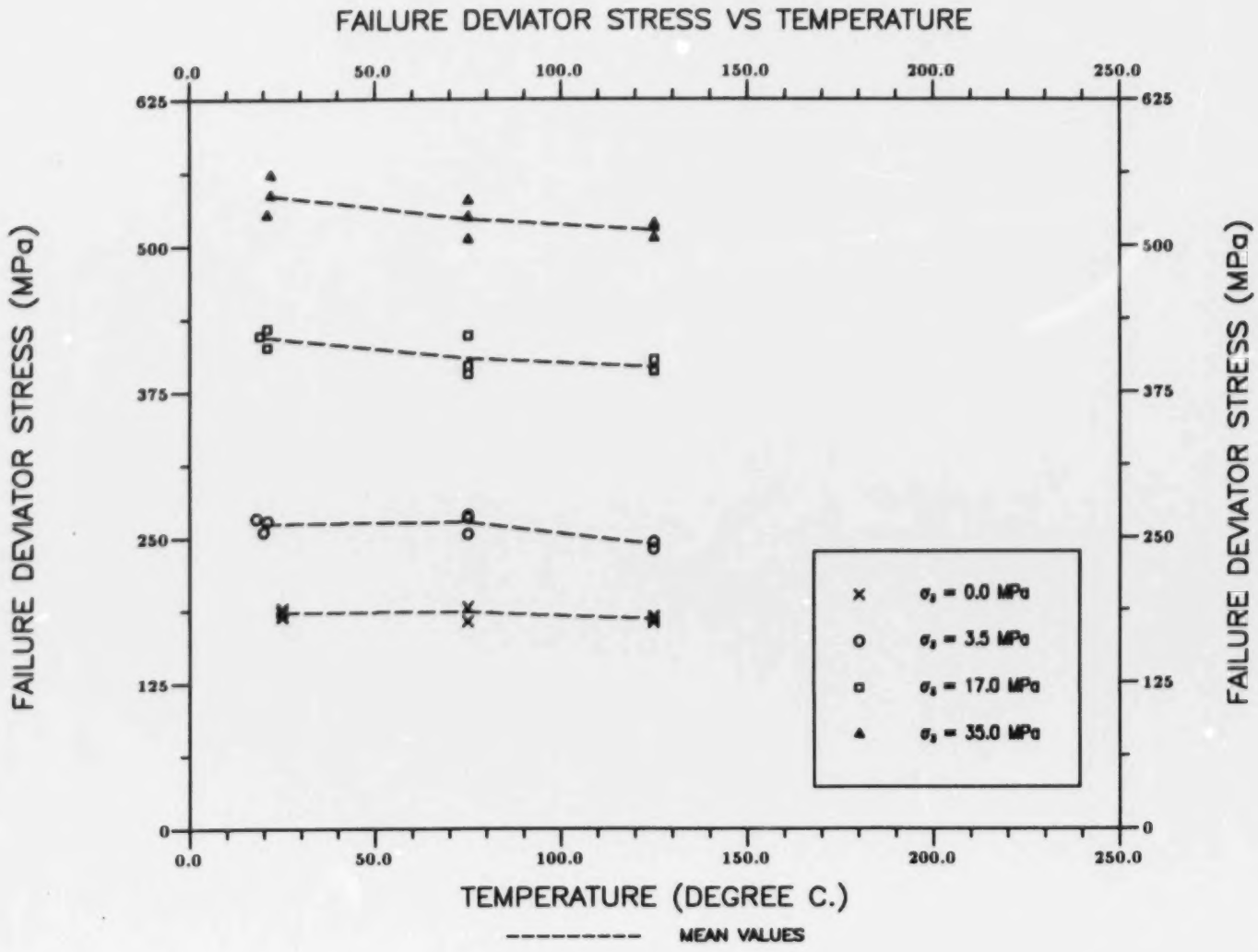

Figure 1. Plots of failure deviator stress versus temperature.

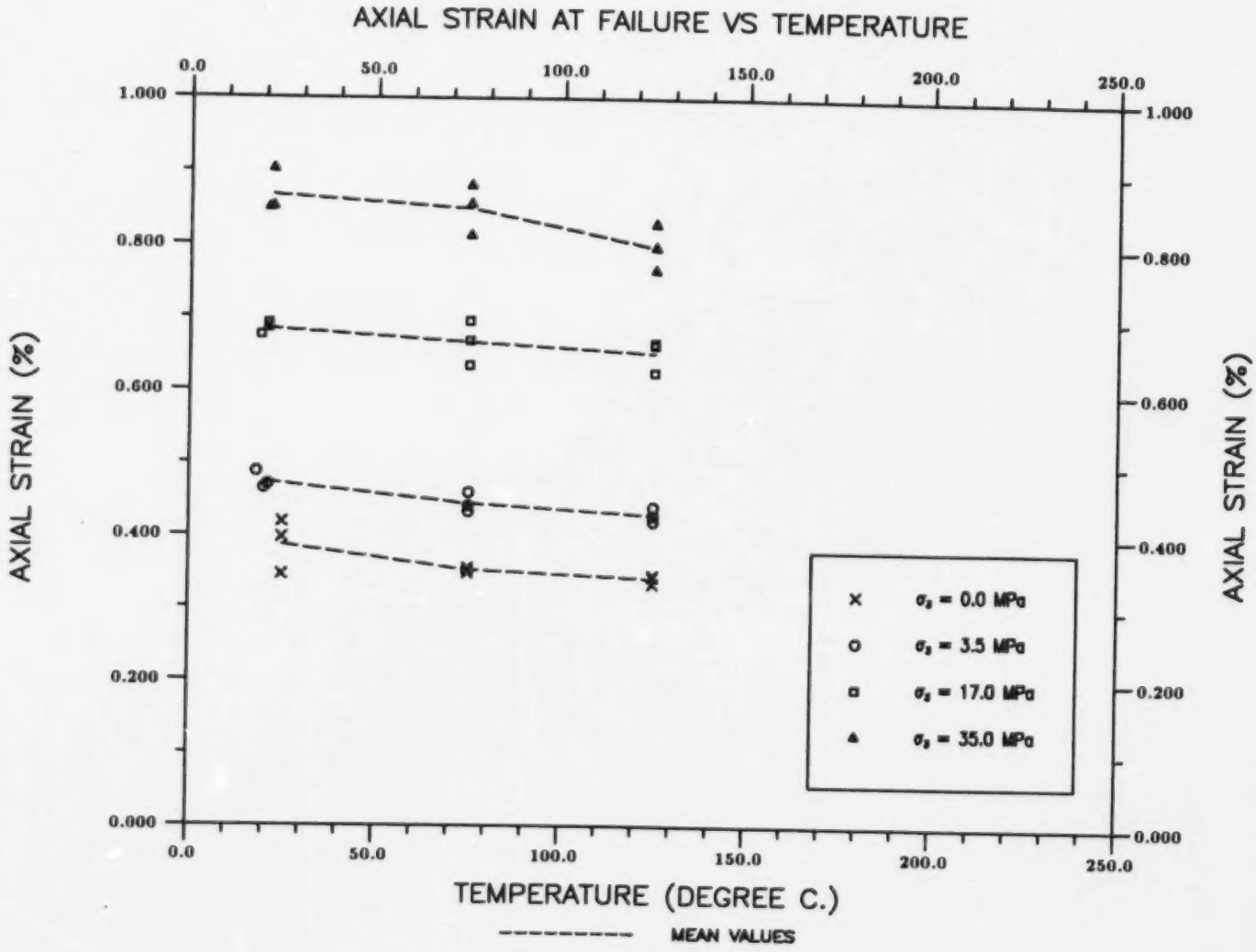

Figure 2. Plots of axial strain at failure versus temperature.

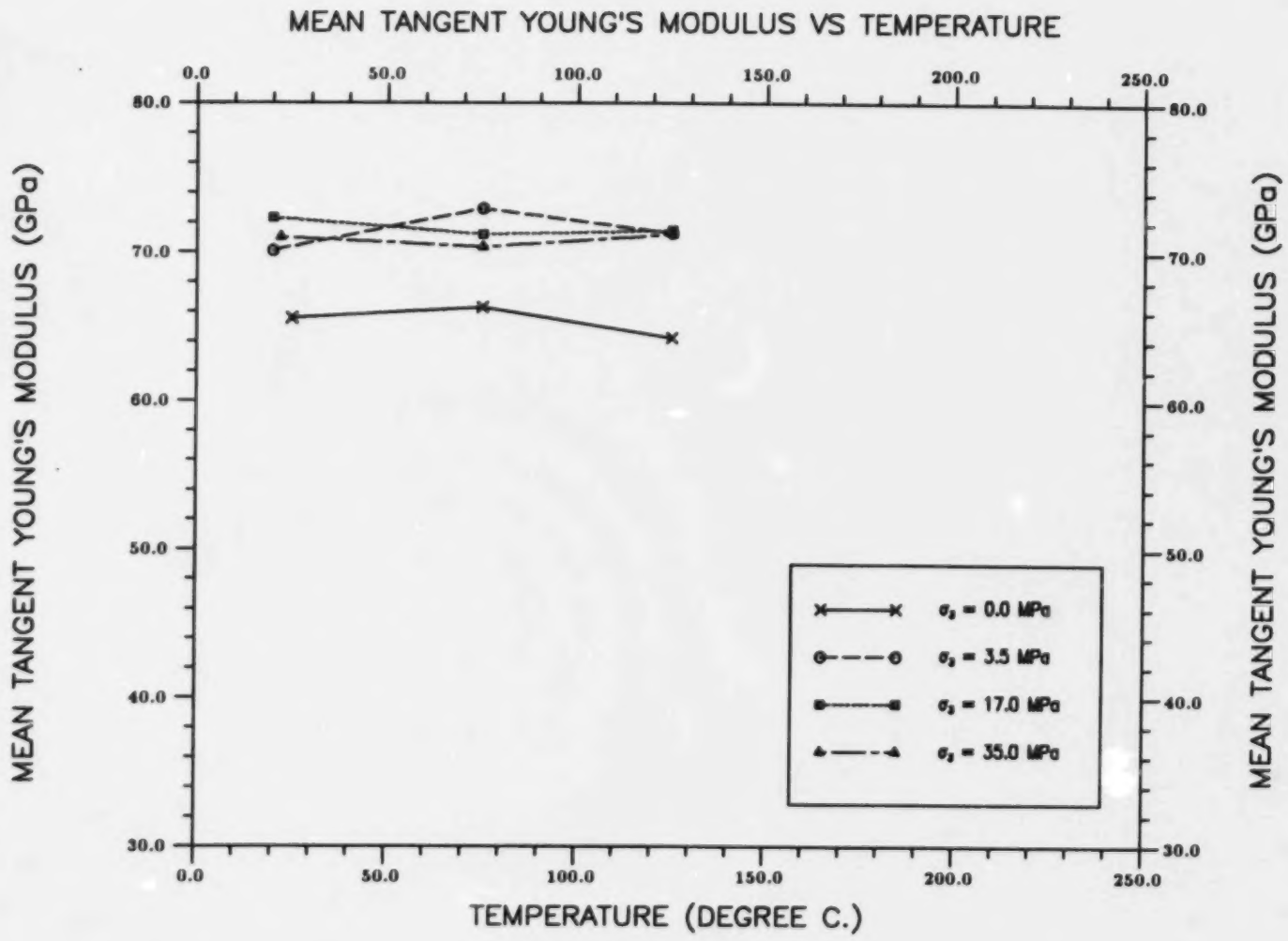

Figure 3. Plots of mean tangent Young's modulus at the stress level of 50 % of $(\sigma_1 - \sigma_3)_f$ versus temperature.

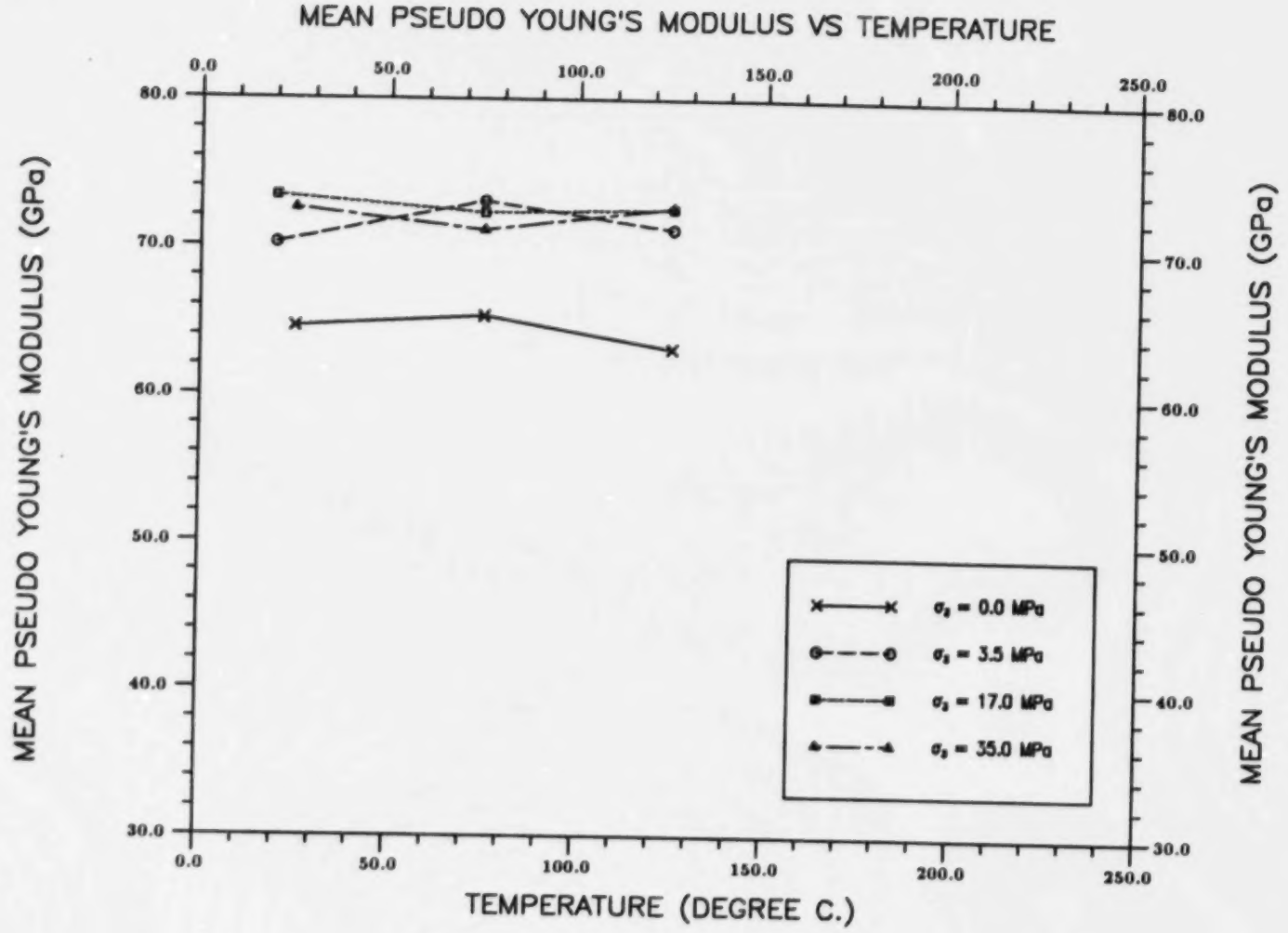

Figure 4. Plots of mean pseudo Young's modulus at the stress level of 50 % of $(\sigma_1 - \sigma_3)_f$ versus temperature.

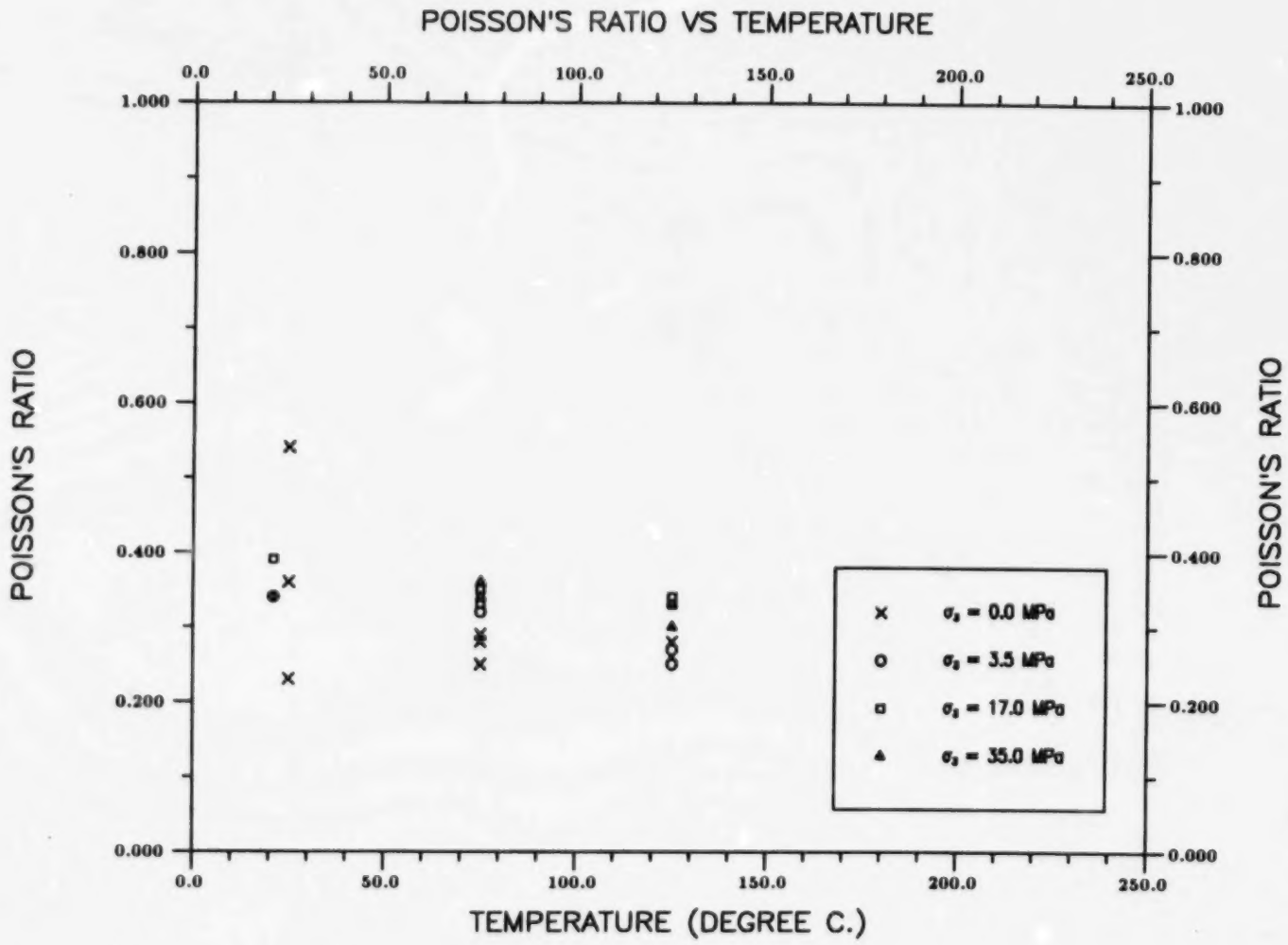

Figure 5. Plots of Poisson's ratio versus temperature.

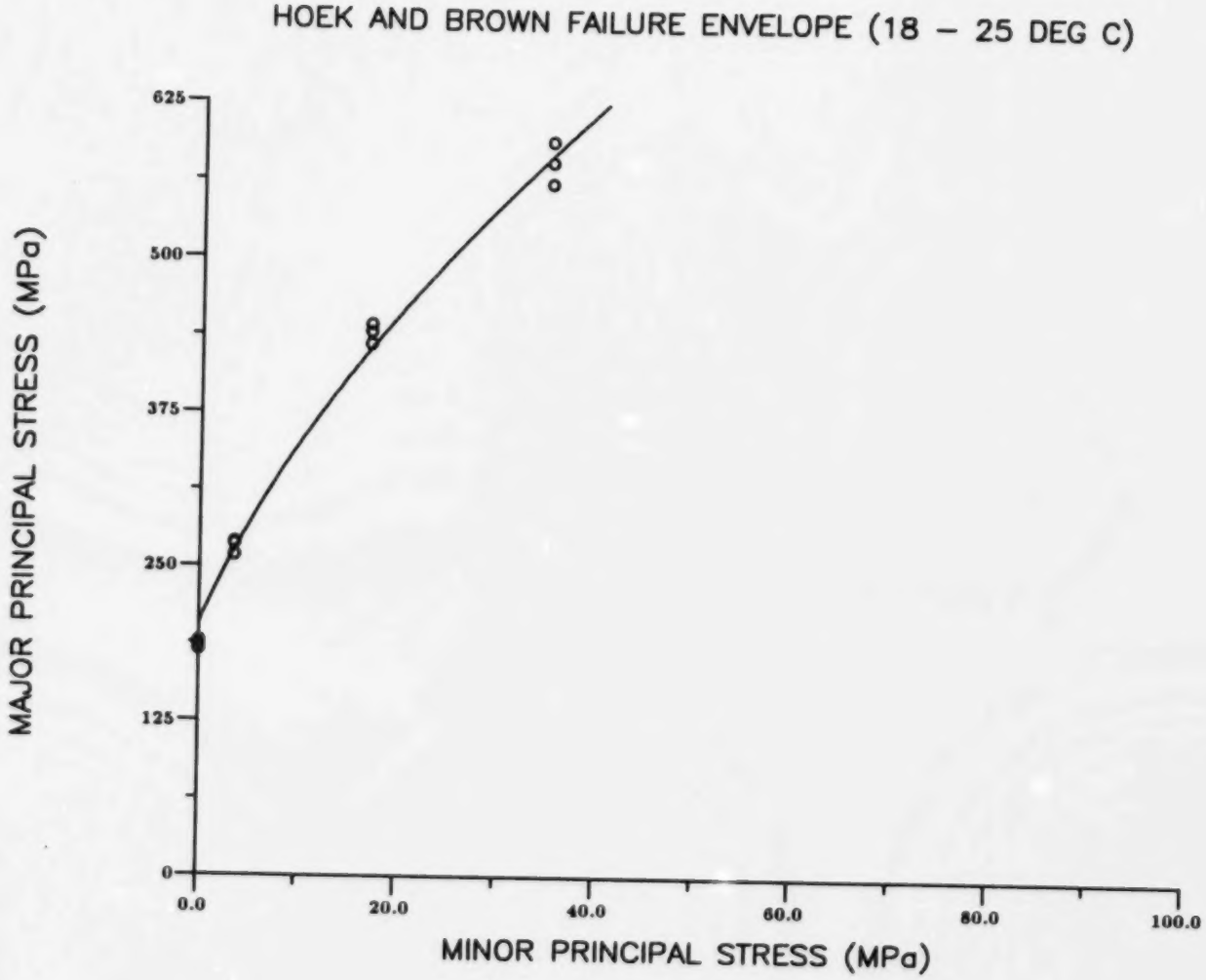

Figure 6. Hoek and Brown failure envelope for tests conducted at 18° – 25° C.

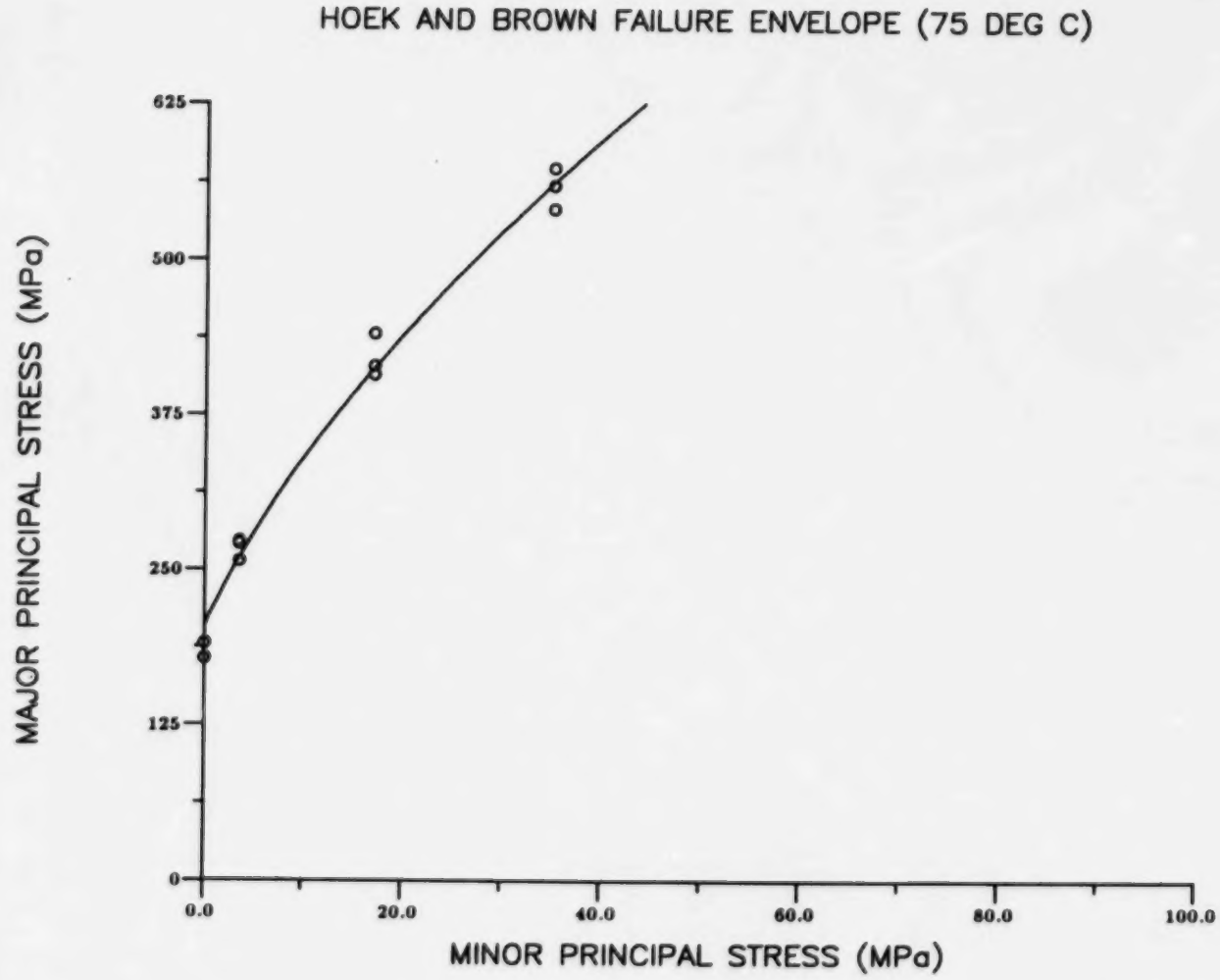

Figure 7. Hoek and Brown failure envelope for tests conducted at 75° C.

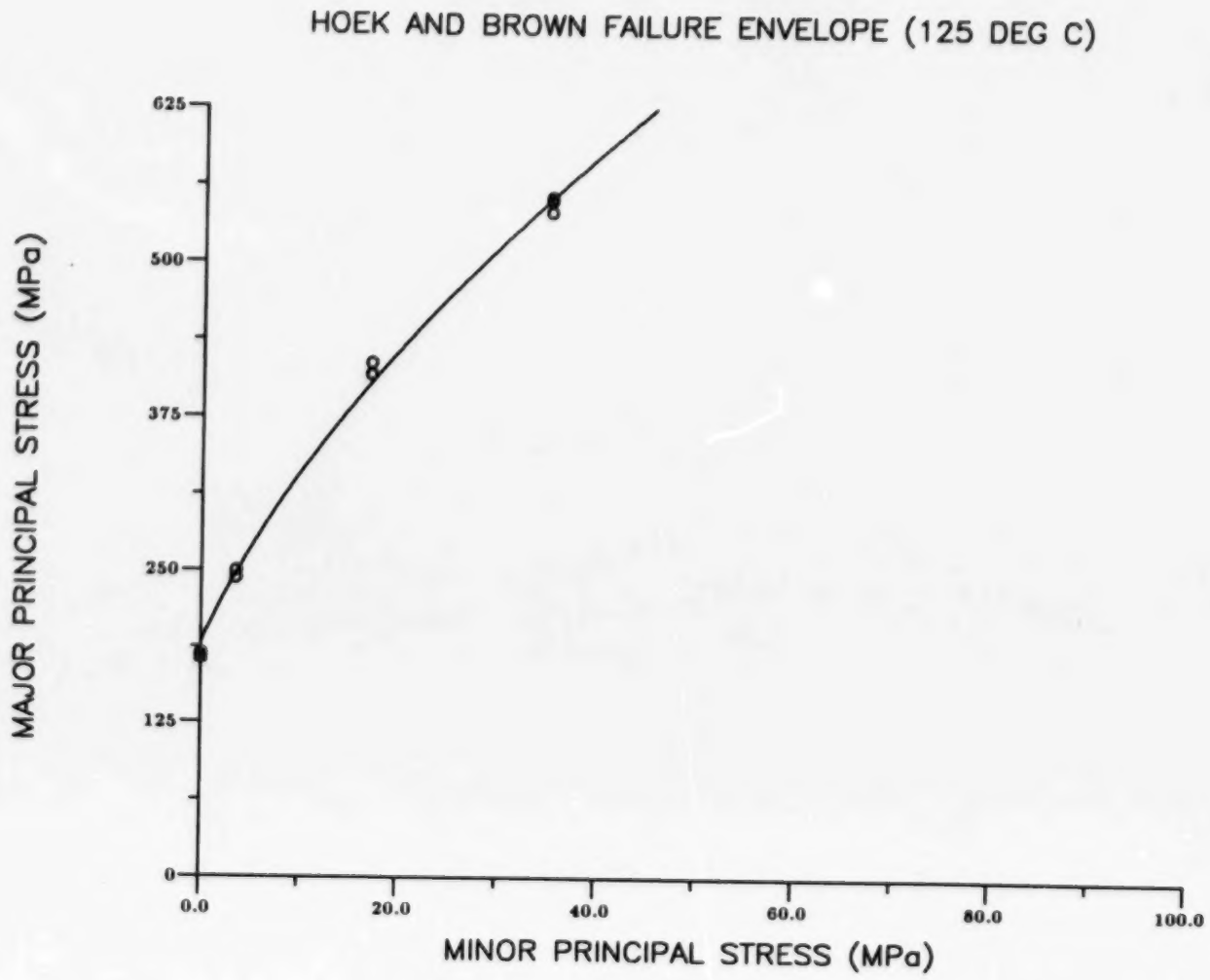

Figure 8. Hoek and Brown failure envelope for tests conducted at 125° C.

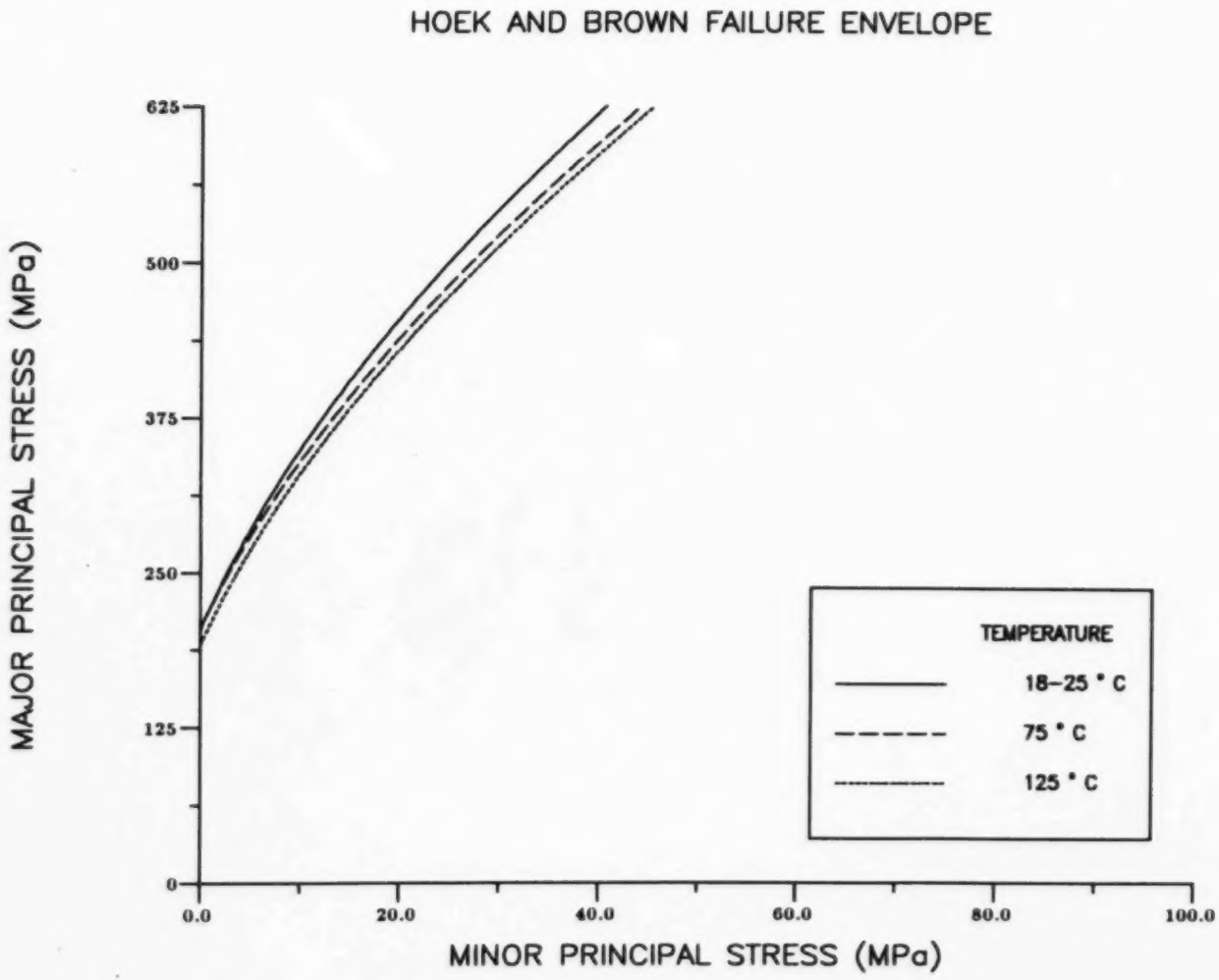

Figure 9. Effect of temperature on the Hoek and Brown failure envelope.

APPENDIX A

Stress-strain Curves for Specimens from
Boreholes 209-021-SV1 and 209-025-SV2

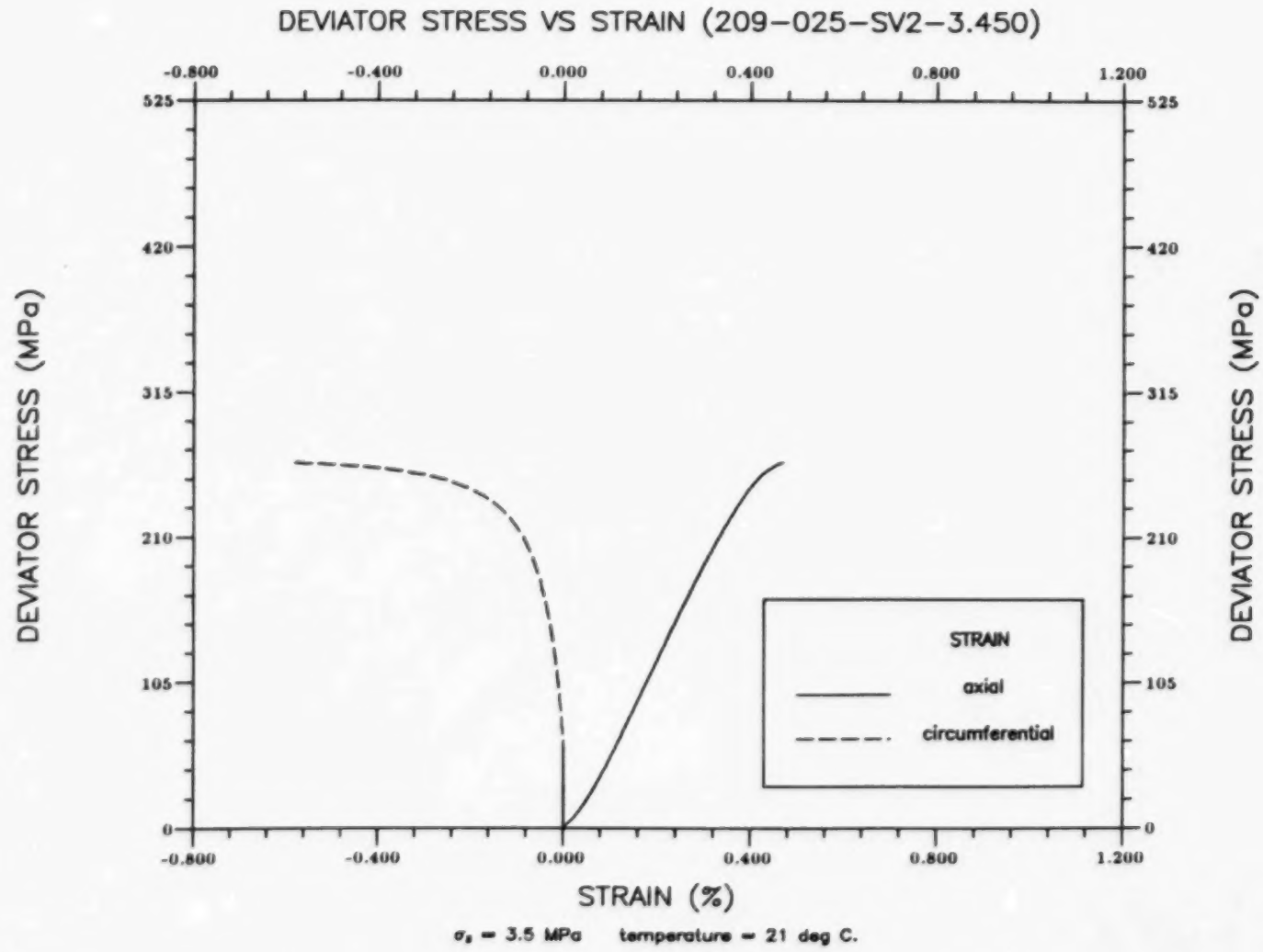

Figure A1. Stress-strain curves for Specimen 209-025-SV2-3.450 tested at 21° C and at $\sigma_3 = 3.5$ MPa.

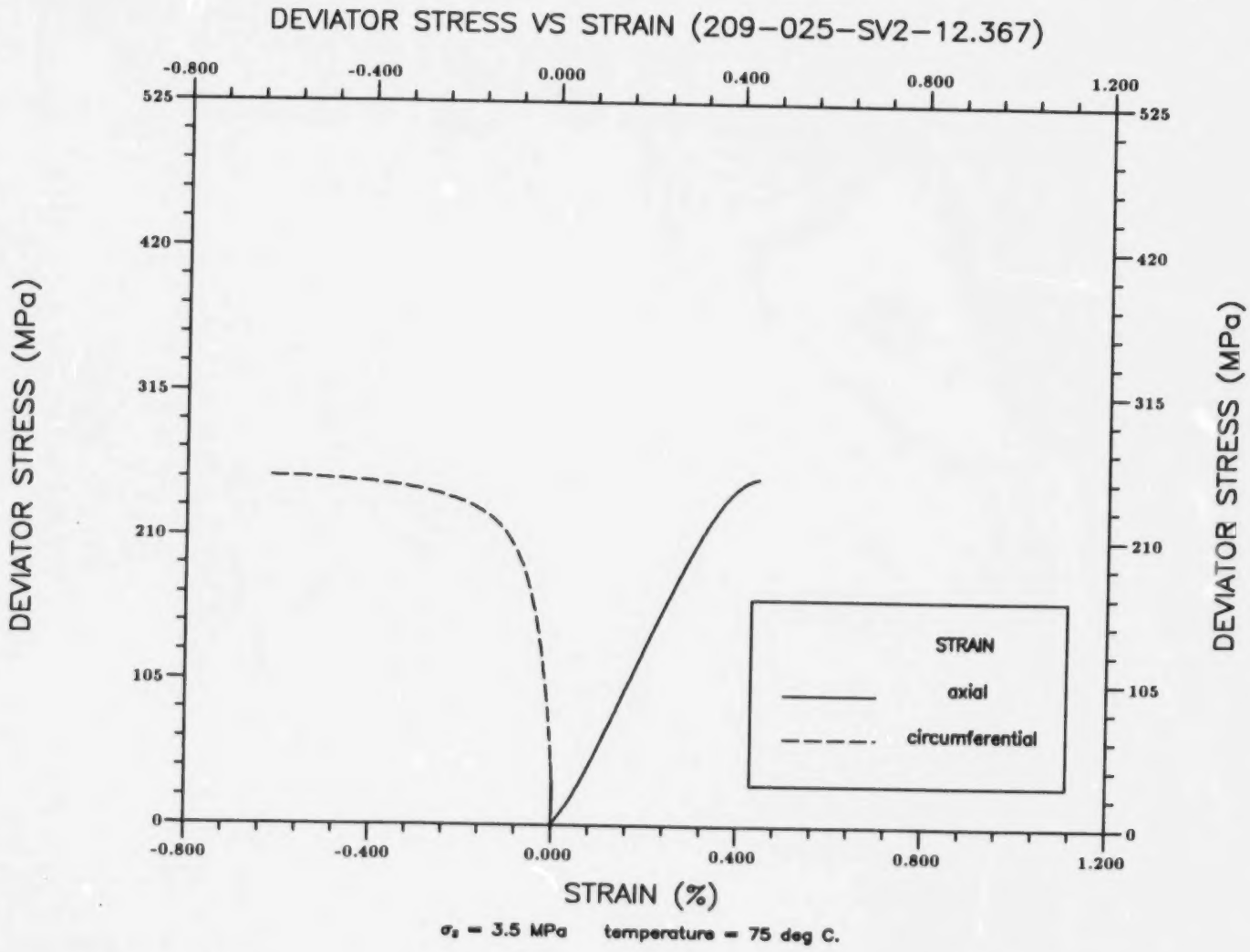

Figure A2. Stress-strain curves for Specimen 209-025-SV2-12.367 tested at 75° C and at $\sigma_3 = 3.5$ MPa.

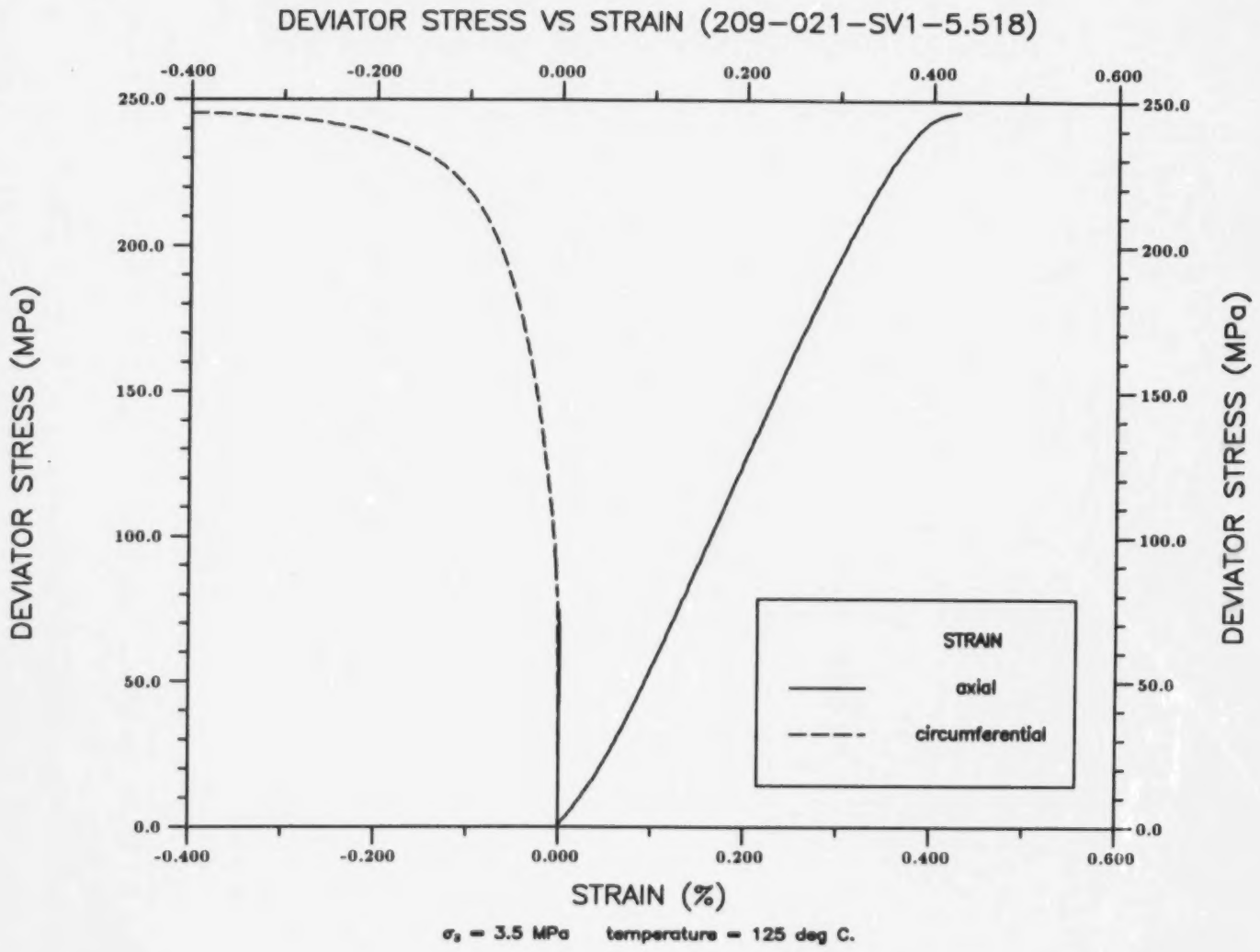

Figure A3. Stress-strain curves for Specimen 209-021-SV1-5.518 tested at 125° C and at $\sigma_3 = 3.5$ MPa.

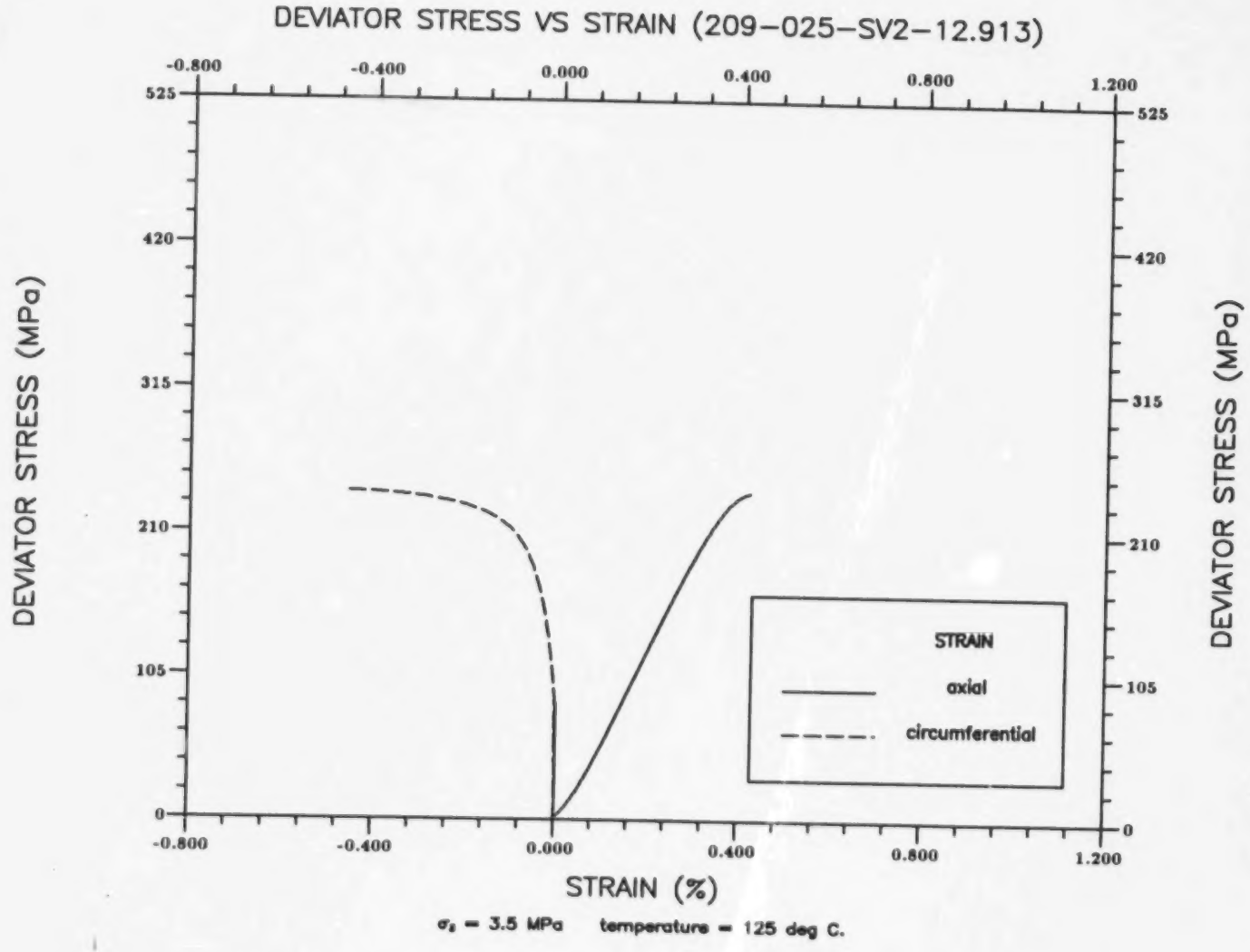

Figure A4. Stress-strain curves for Specimen 209-025-SV2-12.913 tested at 125° C and at $\sigma_3 = 3.5$ MPa.

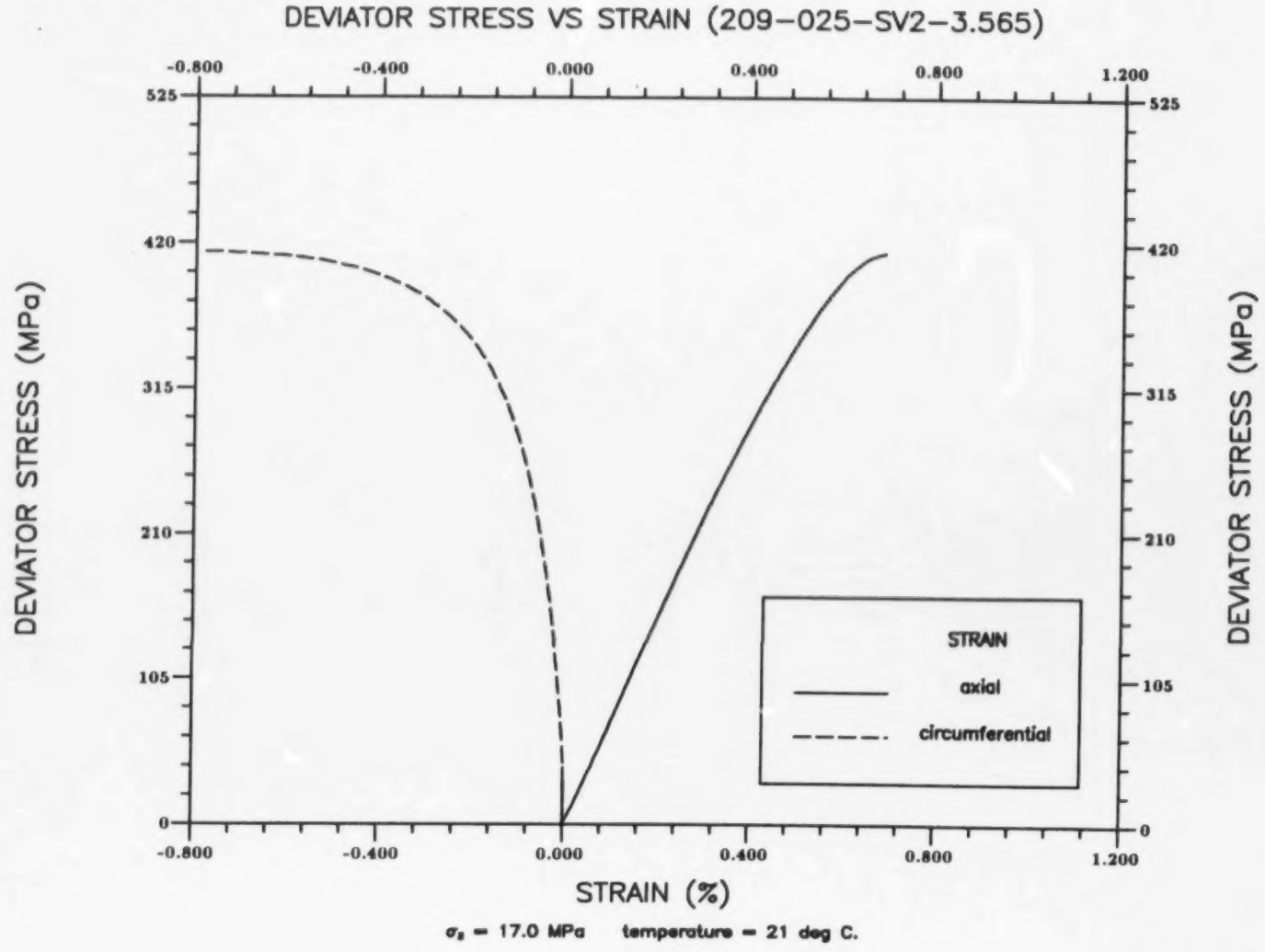

Figure A5. Stress-strain curves for Specimen 209-025-SV2-3.565 tested at 21° C and at $\sigma_3 = 17$ MPa.

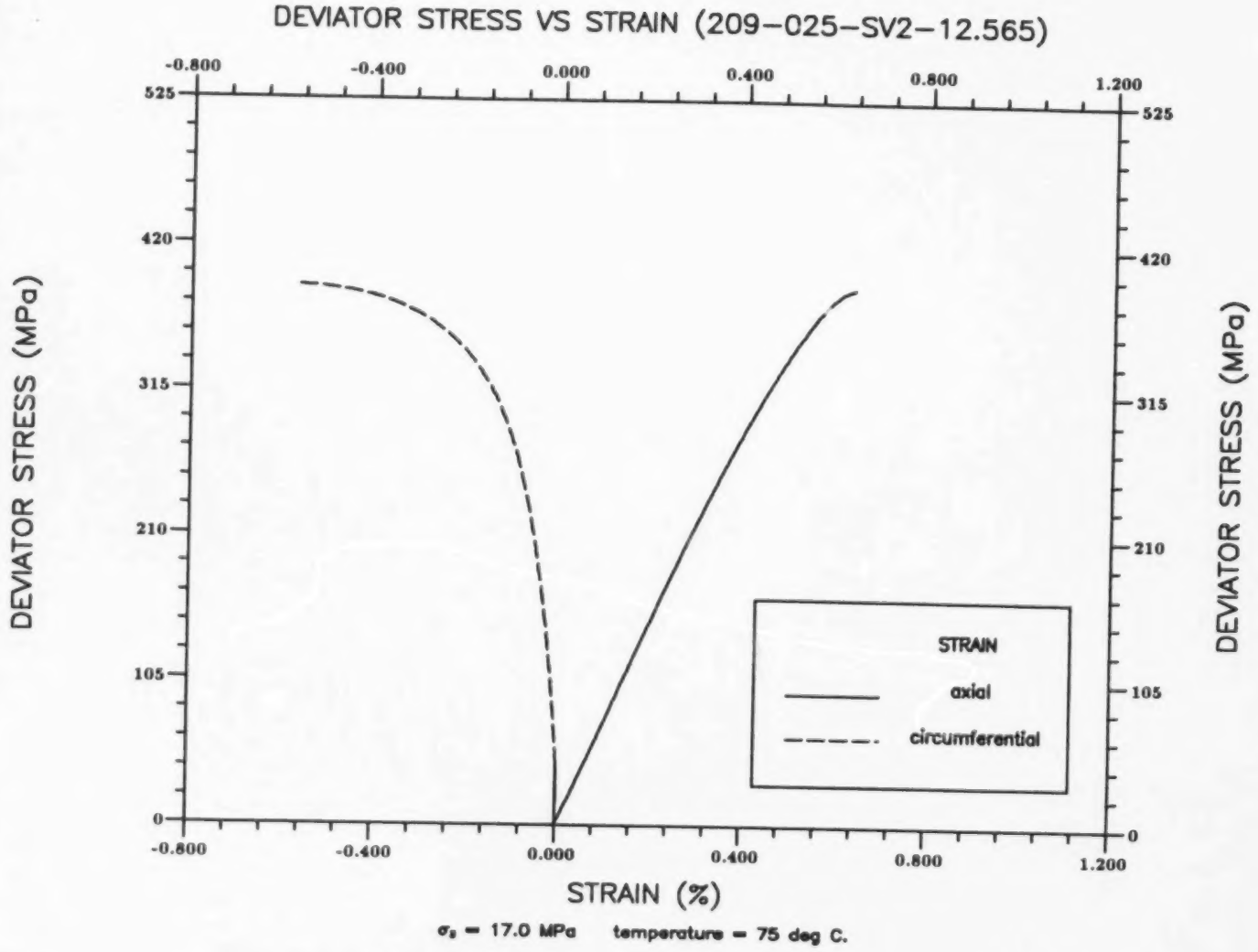

Figure A6. Stress-strain curves for Specimen 209-025-SV2-12.565 tested at 75° C and at $\sigma_3 = 17$ MPa.

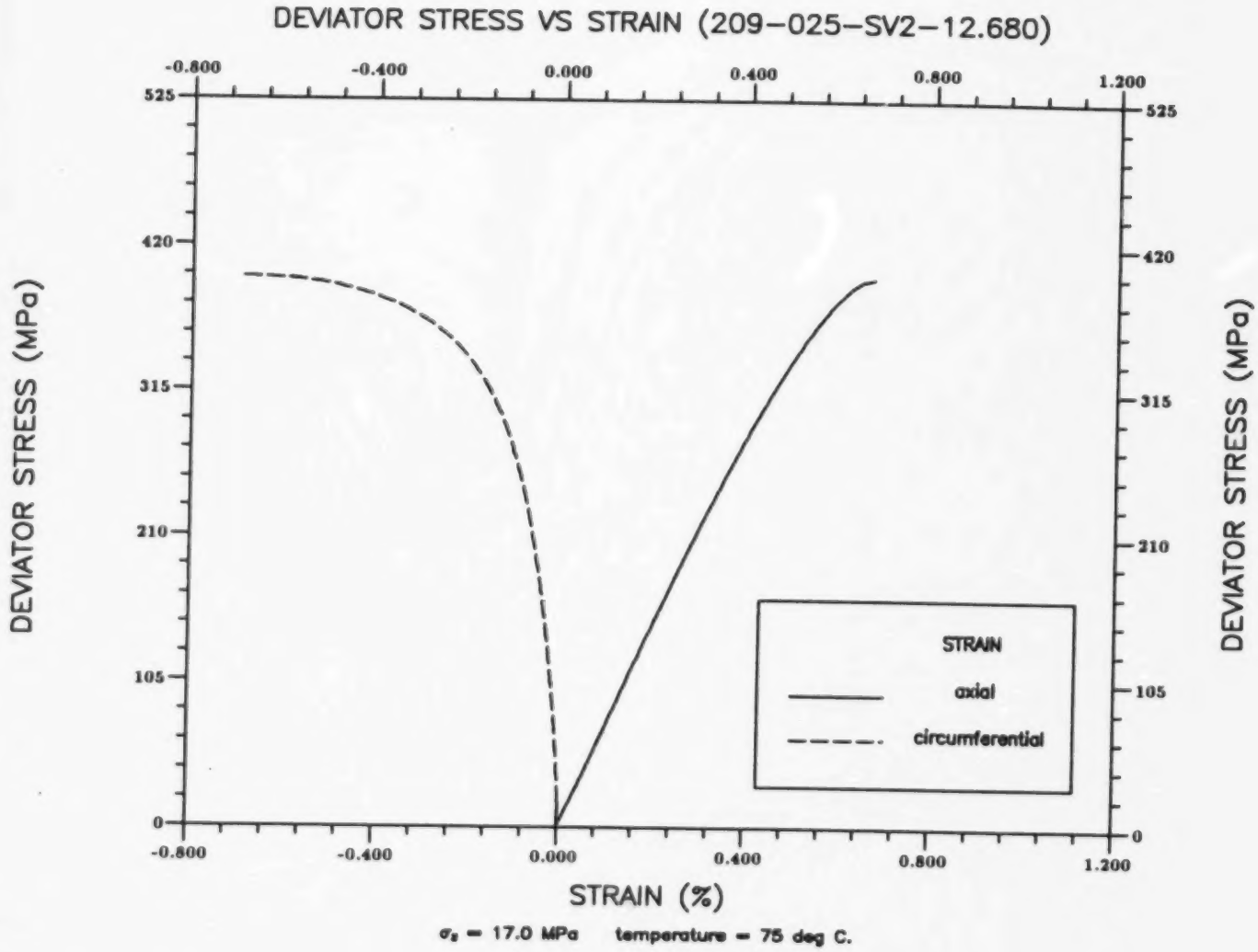

Figure A7. Stress-strain curves for Specimen 209-025-SV2-12.680 tested at 75° C and at $\sigma_3 = 17$ MPa.

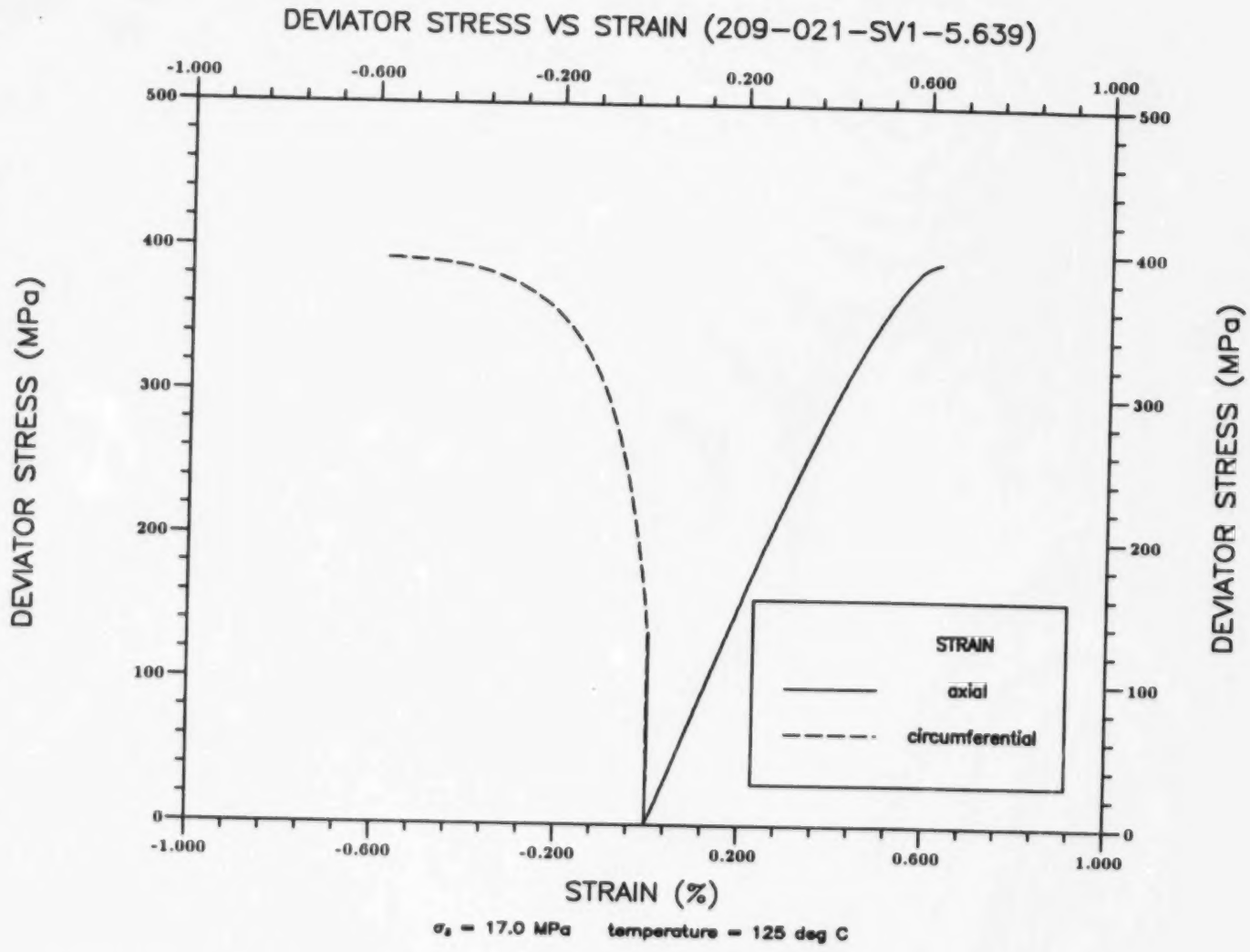

Figure A8. Stress-strain curves for Specimen 209-021-SV1-5.639 tested at 125° C and at $\sigma_3 = 17$ MPa.

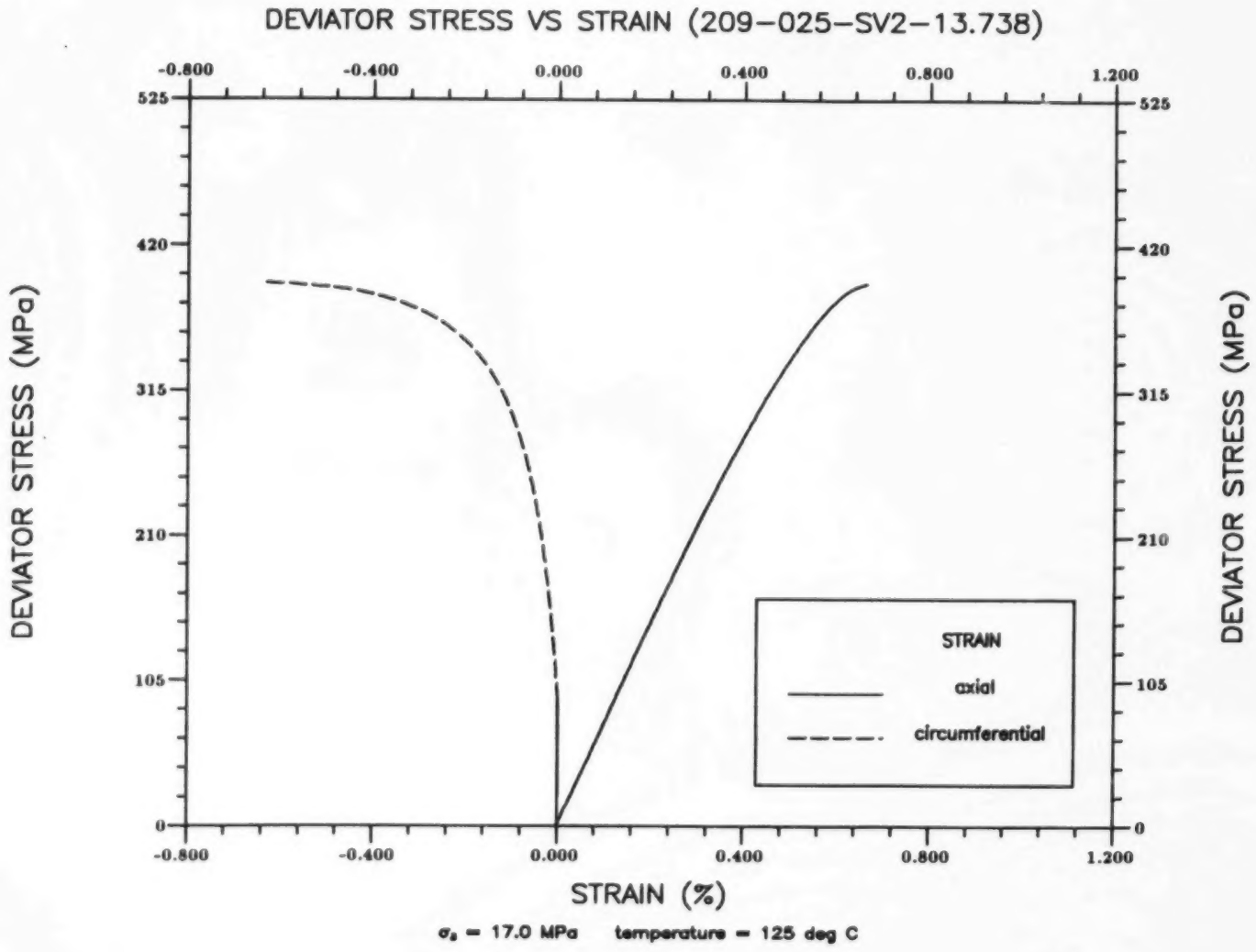

Figure A9. Stress-strain curves for Specimen 209-025-SV2-13.738 tested at 125° C and at $\sigma_3 = 17$ MPa.

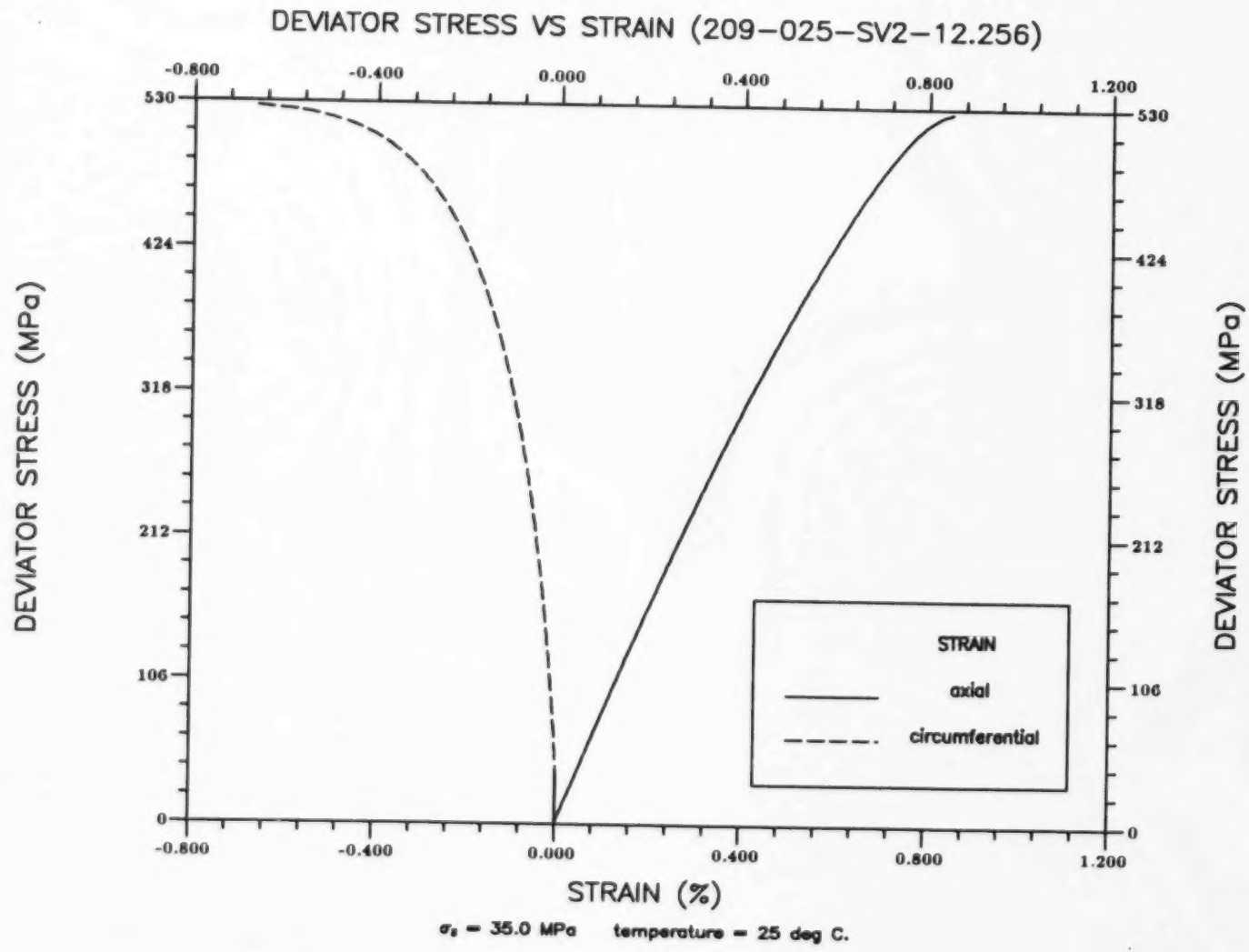

Figure A10. Stress-strain curves for Specimen 209-025-SV2-12.256 tested at 21° C and at $\sigma_3 = 35$ MPa.

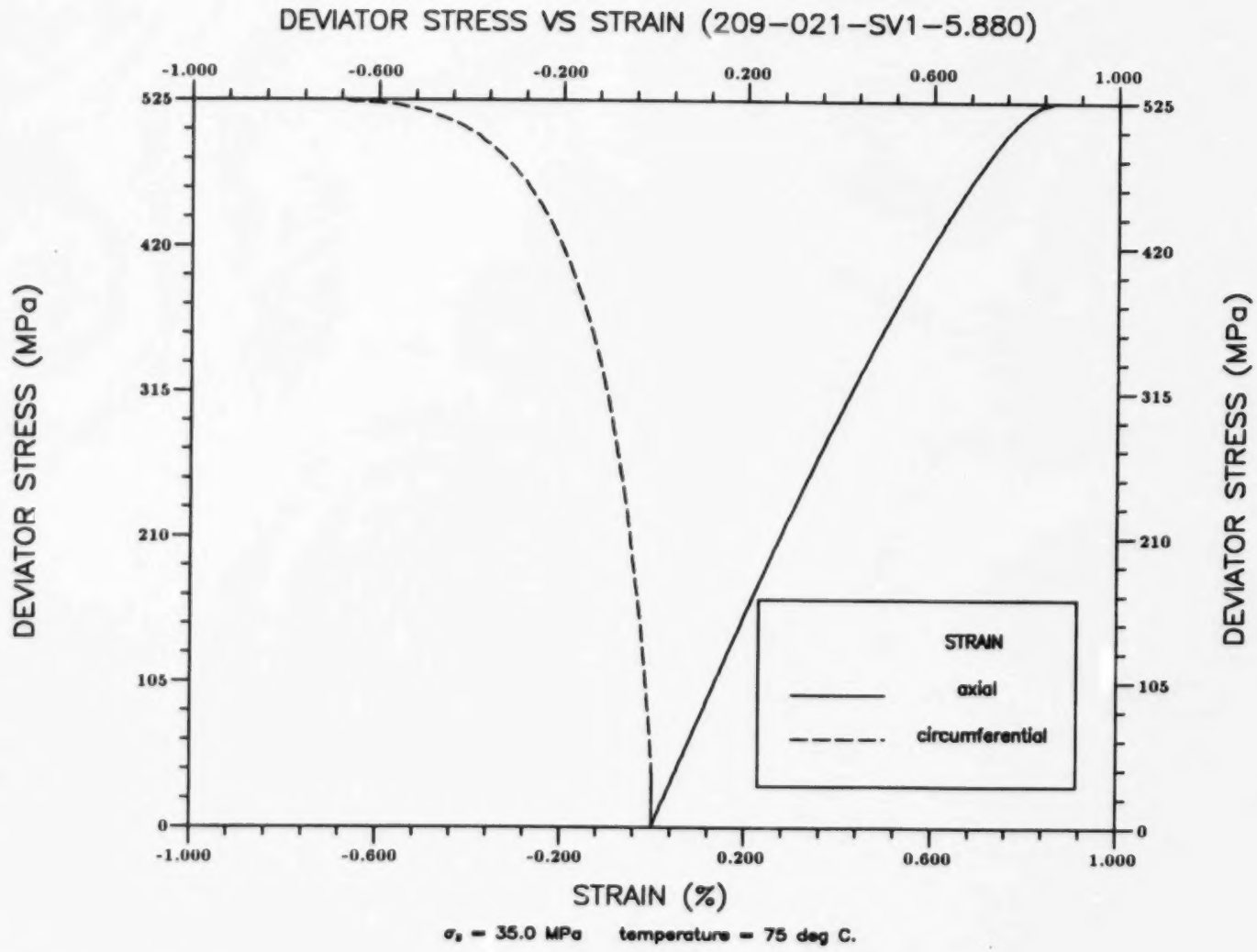

Figure A11. Stress-strain curves for Specimen 209-021-SV1-5.880 tested at 75° C and at $\sigma_3 = 35$ MPa.

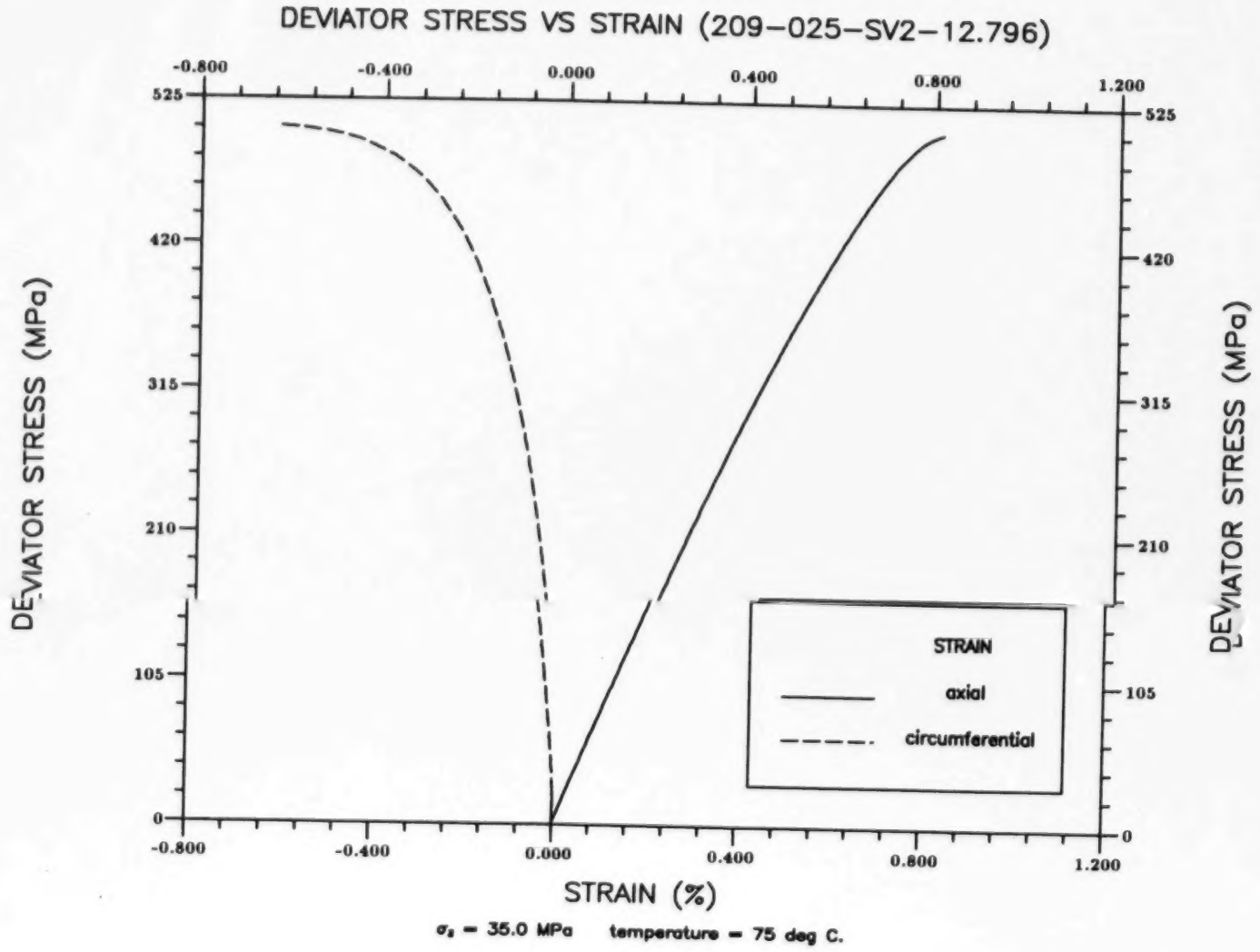

Figure A12. Stress-strain curves for Specimen 209-025-SV2-12.796 tested at 75° C and at $\sigma_3 = 35$ MPa.

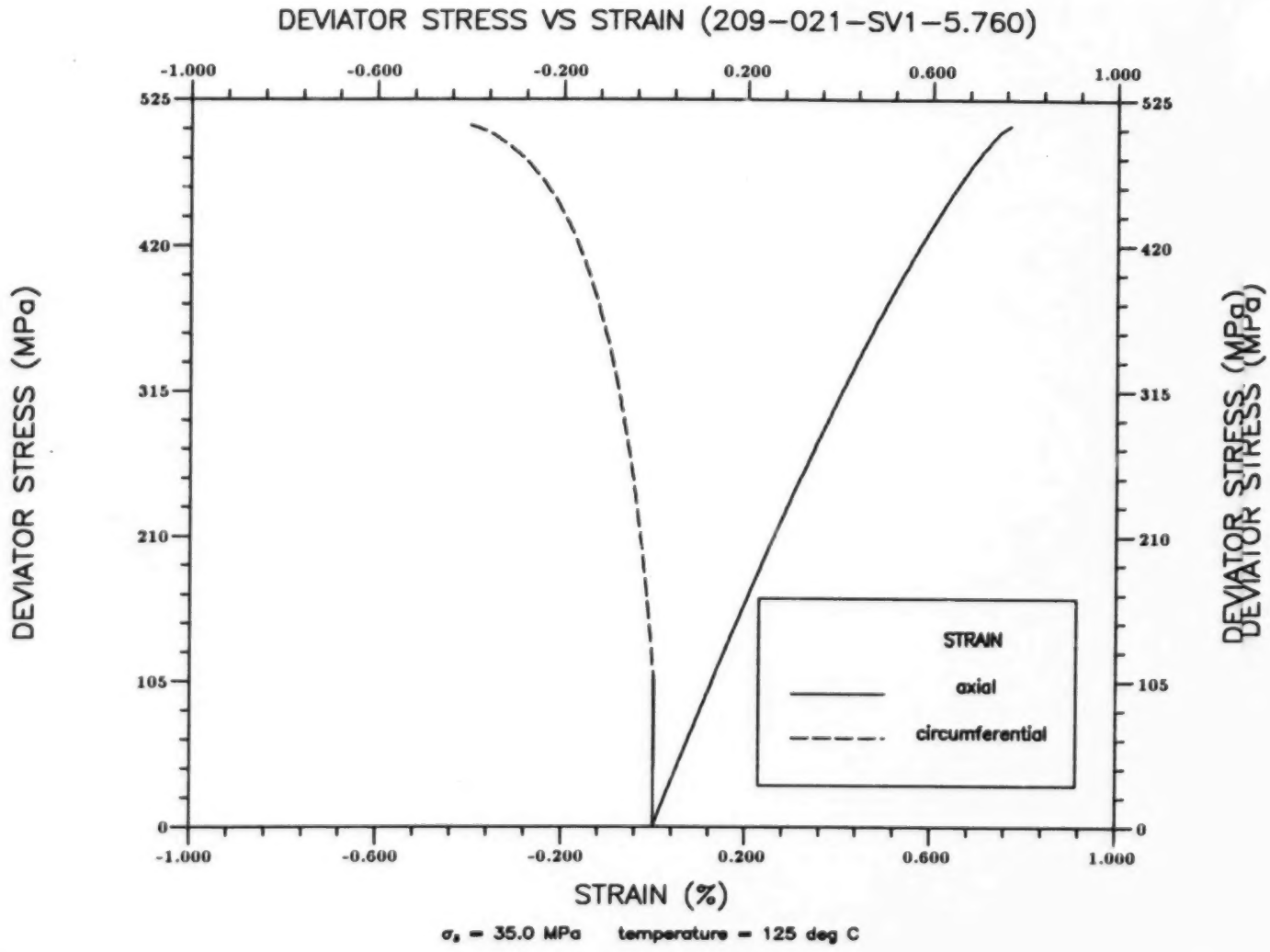

Figure A13. Stress-strain curves for Specimen 209-021-SV1-5.760 tested at 125° C and at $\sigma_3 = 35$ MPa.[a.]

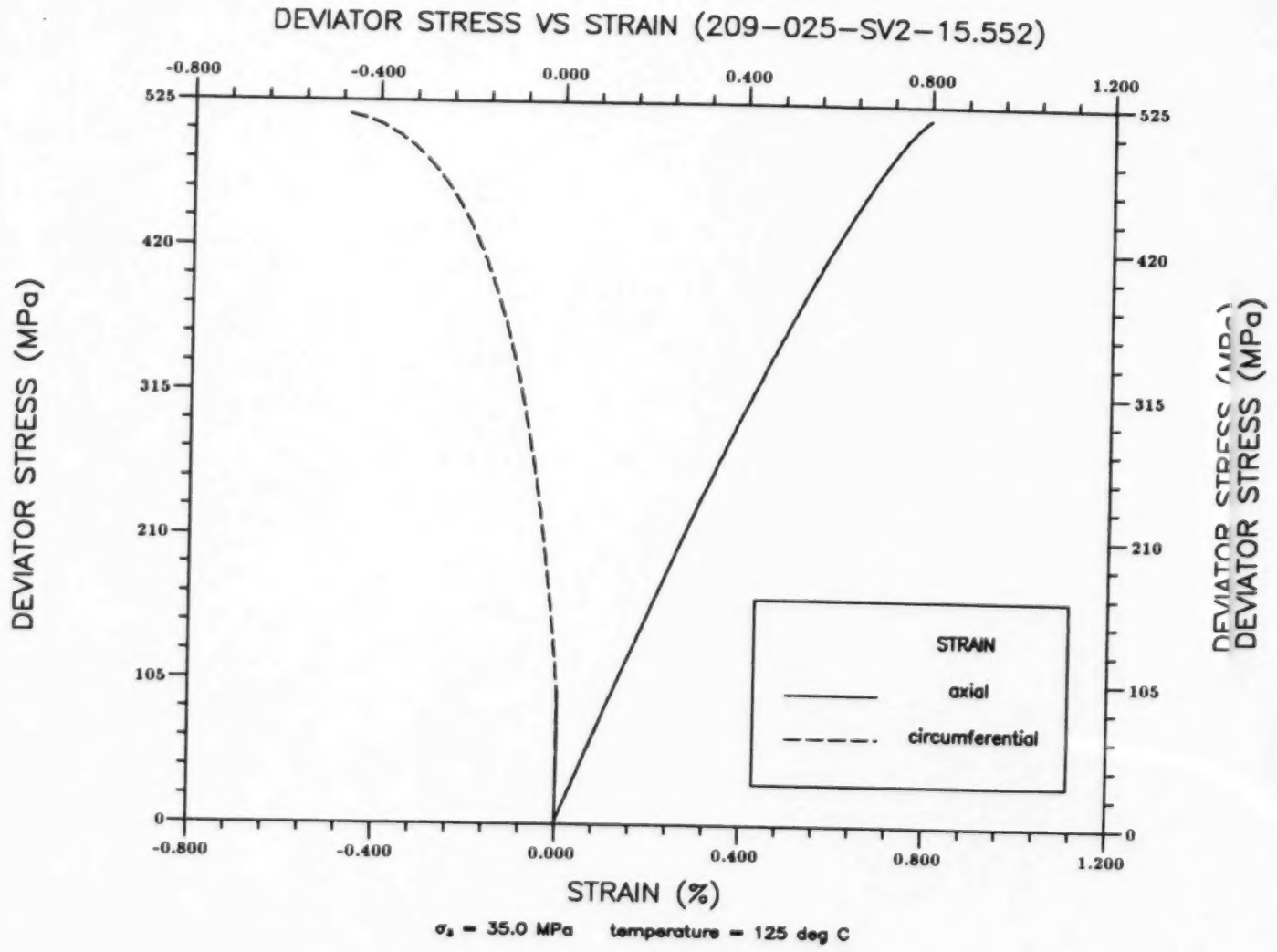

Figure A14. Stress-strain curves for Specimen 209-025-SV2-15.552 tested at 125° C and at $\sigma_3 = 35$ MPaPa.